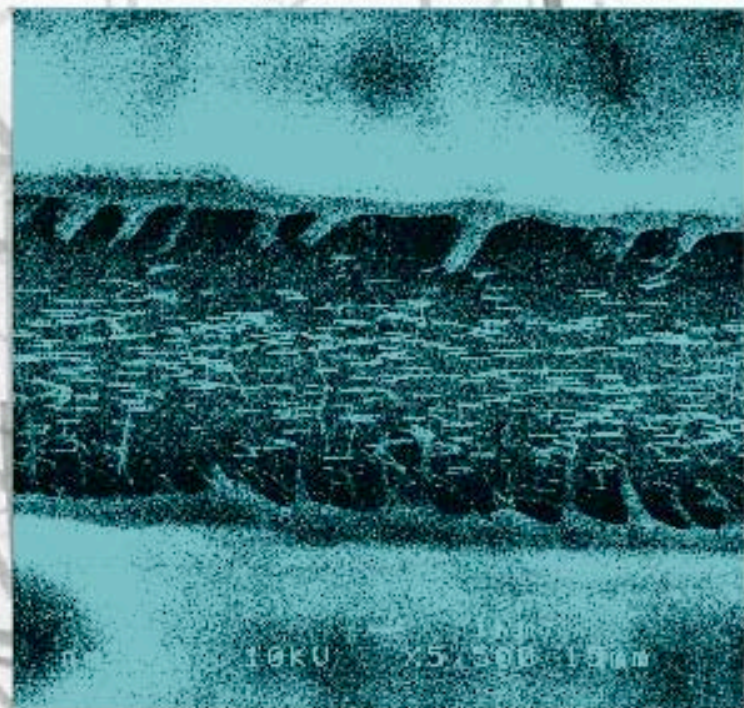


Integration of Nanowires with Microfluidics for Bioapplications

Magnus Jonsson



LUND UNIVERSITY

Master of Science thesis
Spring 2005
Supervisor: Dr. Jonas Tegenfeldt
Solid State Physics
Lund Institute of Technology
Lund University

Integration of Nanowires with Microfluidics for Bioapplications

Master thesis

Magnus Jonsson

Supervisor: Dr. Jonas Tegenfeldt

Division of Solid State Physics
Lund Institute of Technology
Lund University

2005



Abstract

In this master project we have successfully integrated nanowires with microfluidics by flowing buffered DNA through sealed channels containing GaP nanowires. We saw DNA stretching out around single nanowires without damaging them, showing that nanowires are strong enough to act as nanometer-sized features in future applications. Several methods were tested, of which these three were most successful:

- fabrication of SU8 channels around GaP nanowires grown on GaP and bonding to a piece of glass covered with PMMA
- fabrication of SU8 channels around GaP nanowires grown on GaP and bonding to PDMS after oxygen ashing
- Growth of GaP nanowires in etched Si channels and subsequent oxygen bonding to PDMS

Further, we have managed to grow straight GaP nanowires in etched GaP channels. Studies of growth in etched Si channels show nanowires grown in all directions, which we believe could be positive for specific applications. In addition, we suggest several future bioapplications to emphasise the importance of this work.

Acknowledgement

I would like to thank everyone at the department for being friendly, helpful and for interesting discussions. Extra credit to:

My supervisor Jonas Tegenfeldt for all ideas and feedback. Prof. Lars Samuelsson for giving me the opportunity to work with nanowires. Prof. Fredrik Höök for introducing me to the biogroup. Ivan Maximov for teaching me the SEM and wet etching. David Adolph for teaching me how to operate the AFM, RIE and PECVD and also interesting discussions. Patrick Carlberg and Jason Beech for teaching me the lithography process. Mariusz Graczyk for making masks, discussions and help with evaporation and PECVD. Thomas Mårtensson and Kimberly Dick for growing nanowires and nanotrees and for your knowledge about growth and stuff. Brent Wacaser and Patrick Svensson for information and helpful discussions. Per-Olof Larsson for information about plasmids and supercoiled DNA.

Acronyms and Abbreviations

1D	Three-dimensional
2D	Two-dimensional
3D	Three-dimensional
AFM	Atomic Force Microscopy
Ag	Silver
Au	Gold
CVD	Chemical Vapour Deposition
EBL	Electron Beam Lithography
GaAs	Gallium Arsenide
GaP	Gallium Phosphide
HF	Hydrofluoric acid
MEMS	Micro Electro Mechanical Systems
MetOH	Methanol
MOVPE	Metal-Organic Vapour Phase Epitaxy
NIL	Nanoimprint Lithography
PDMS	Poly(dimethylsiloxane)
PECVD	Plasma Enhanced Chemical Vapour Deposition
RF	Radio Frequency
RIE	Reactive Ion Etching
SEM	Scanning Electron Microscopy
Si	Silicon
SiN	Silicon Nitride (non stoichiometric)
SiO	Silicon Mono Oxide
SiO _x	Silicon Oxide (non stoichiometric)
SPR	Surface Plasmon Resonance
SOG	Spin On Glass
SPM	Scanning Probe Microscopy
VLS	Vapour Liquid Solid
VPE	Vapour Phase Epitaxy

Contents

ABSTRACT	III
ACKNOWLEDGEMENT	V
ACRONYMS AND ABBREVIATIONS	VII
CONTENTS	IX
1. INTRODUCTION.....	1
1.1 THE IMPORTANCE OF THE PROJECT	1
1.1.1 <i>Scaling down</i>	1
1.1.2 <i>Working in water</i>	2
1.1.3 <i>Combining nanowires and microfluidics</i>	2
1.2 THREE IDEAS OF CHANNEL STRUCTURES AROUND NANOWIRES	3
2. THEORY	5
2.1 MICROFLUIDICS	5
2.1.1 <i>Introduction</i>	5
2.1.2 <i>Fluids and the Navier-Stokes equations</i>	5
2.1.3 <i>Turbulent and Laminar flows</i>	6
2.1.4 <i>Pressure driven flows in small channels</i>	6
2.1.5 <i>Capillary driven flows</i>	8
2.2 <i>Nanowires</i>	9
2.2.1 <i>Epitaxy</i>	10
2.2.2 <i>MOVPE-Metal-Organic Vapour Phase Epitaxy</i>	10
2.2.3 <i>The Vapour Liquid-Solid Model</i>	11
2.2.4 <i>The Vapour Solid-Solid Model</i>	11
2.3 FABRICATION	12
2.3.1 <i>Bonding by Oxygen ashing</i>	12
2.3.3 <i>UV-lithography</i>	13
2.3.4 <i>Plasma Enhanced Chemical Vapour Deposition (PECVD)</i>	13
2.3.5 <i>Thermal Evaporation of Silicon Oxide</i>	14
2.3.6 <i>Reactive ion etching (RIE)</i>	15
2.3.7 <i>Wet etching</i>	15
2.3.8 <i>PDMS molding</i>	16
2.4 IMAGING TECHNIQUES	16
2.4.1 <i>Atomic Force Microscopy</i>	16
2.4.2 <i>Scanning Electron Microscopy</i>	18
2.4.3 <i>Epifluorescence Microscopy</i>	18
3. GENERAL BONDING EXPERIMENTS.....	21
3.1 OXYGEN PLASMA BONDING	21
3.2 BONDING IN NIL MACHINE	22
4. INTEGRATING NANOWIRES AND MICROFLUIDICS.....	27
4.0 <i>Experimental setup for flowing DNA in channels</i>	27
4.1 CHANNELS ON THE RECIPROCAL SUBSTRATE	28

4.2 CONSTRUCTION OF CHANNELS AROUND NANOWIRES	29
4.4 GROWTH OF NANOSTRUCTURES IN ETCHED TRENCHES	33
4.4.0 Choice of materials	33
4.4.1 Growing nanowires in etched gallium phosphide channels	34
4.4.2 Growing GaP nanowires in etched silicon channels	39
5. CONCLUSION.....	43
6. OUTLOOK	45
6.1 GROWTH OF BRANCHED NANOSTRUCTURES IN ETCHED SILICON CHANNELS	45
6.1.1 Method no.1.....	45
6.1.2 Method no.2.....	45
6.2 FUTURE APPLICATIONS	47
6.2.1 Novel topological separator for DNA	47
6.2.2 Protein separator - Bumper array.....	48
6.2.3 Biosensor using oscillating nanowires.....	49
6.2.4 Surface area enhancer.....	49
7. REFERENCES.....	51
APPENDIX A-PROCESSING PARAMETERS AND RECIPES.....	53
Recipe for Photolithography with Shipley S1813	53
Recipe for Photolithography with SU8.....	53
Recipe for wet etching with Bromine water	54
Recipe for wet etching with Br:MetOH	54
Parameters for PECVD of Silicon Nitride	55
Parameters for RIE in Silicon Nitride	55
Parameters for RIE in silicon.....	55
Recipe for bonding with Nanoimprint machine	56
Recipe for DNA buffer	56
APPENDIX B.....	57
DIFFERENTIAL REPRESENTATION OF FLUID FLOW	57
The Continuity equation	57
The Navier-Stokes equations	58

1. Introduction

1.1 The importance of the project

The aim of this project was to integrate nanowires with microfluidics and in this section I will explain why this is an important step for Science and for Biophysics in particular.

1.1.1 Scaling down

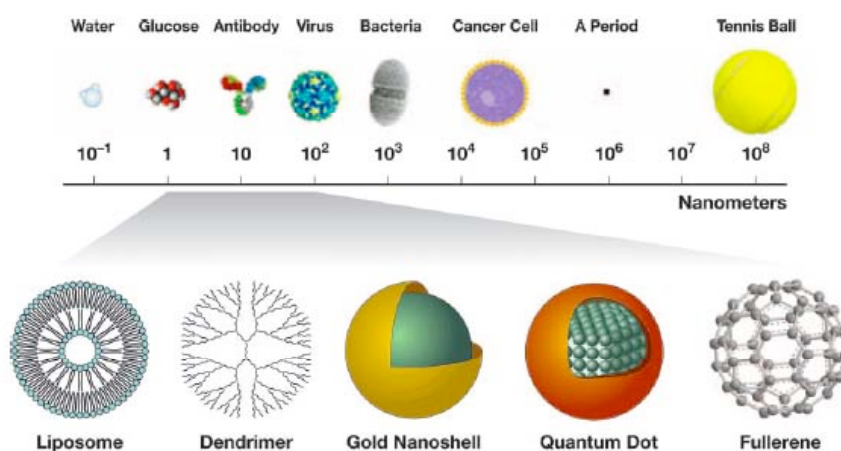


Figure 1.1: Sizes for different types of biomolecules and larger things, such as a typed period. Figure taken from “Nanotechnology for the biologist” by Scott E. McNeil.

These days, the trend is to make things as small as possible. People want smaller and faster computers, small mp3 players with lots of memory and tiny mobile phones with cameras and other built in applications. Even possible exceptions, such as computer screens, which we want to be big, should then instead be as thin as a possible and very light weighted. This push from industry for smaller and better electronic devices is considerable, however there are also other reasons why scaling things down in size is important for Science.

Today we are able to detect, measure and build things on the nanometer scale, which is the same size scale Life itself has chosen to work on after billions of years of Evolution via natural selection. To work on the same scale as Nature makes it promising for us to gain understanding about fundamental biological and biophysical phenomena. [1] With this knowledge and nanometer tools we can improve our ability to mimic these phenomena and this will lead to new kinds of applications. Further, we can address even more fundamental questions, such as why life chose this nanometer size scale in the first place.

Biological and medical applications also demand down scaling. We want to decrease sample volumes, separate smaller particles, probe smaller areas and detect fewer molecules. These requirements are important steps for applications such as lab-on-a-chip devices or micro arrays for detecting protein expression in a small blood sample or perhaps a combination.

1.1.2 Working in water

Biomolecules live in cells in an aqueous environment, on which their properties and functions, such as three dimensional structure and charge, are dependent. External effects such as viscosity do not only affect the properties of the molecules directly, but also their motion and distances between molecules, which affect for example reaction rates. It is thus essential to study biological processes in their natural aqueous environment to ensure that they behave normally.

1.1.3 Combining nanowires and microfluidics

Nanowires are epitaxially grown pillars with diameters of tens of nanometers (nanowires and their growth are described in section 2.2) and length in the micrometer range. Positions and dimensions are controllable and preferred nanostructures can be fabricated. [2, 3] This, together with their high aspect ratio and high stability, make them suitable as nanostructures in microfluidic devices. Promising is also that magnetic and electrical properties are increasingly controlled and that new kinds of heterostructures are invented, such as pn-junctions, core/shell nanowires and hollow tubes [4, 5] and also branched structures such as various types of nanotrees. [6, 7]

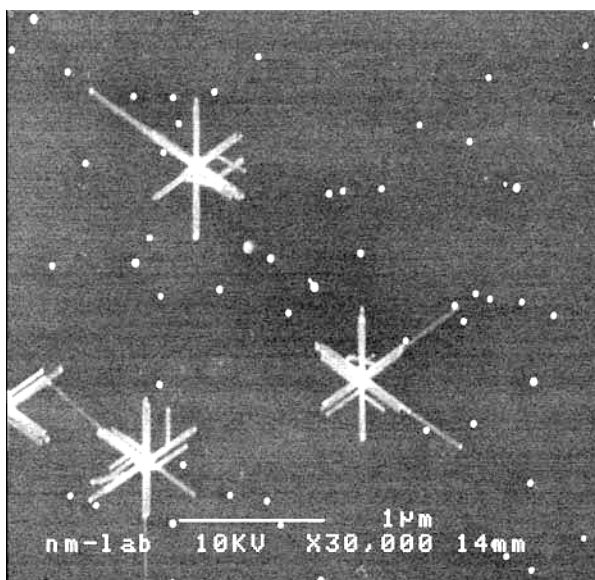


Figure 1.2: A SEM image of nanotrees from above, grown on GaP.

The ability to combine micro/nano-fluidics and nanowires will allow studies in an aqueous environment using the versatility of these nanostructures and at the same time, we can scale down in size considerably. This will lead to new kinds of biological and medical applications.

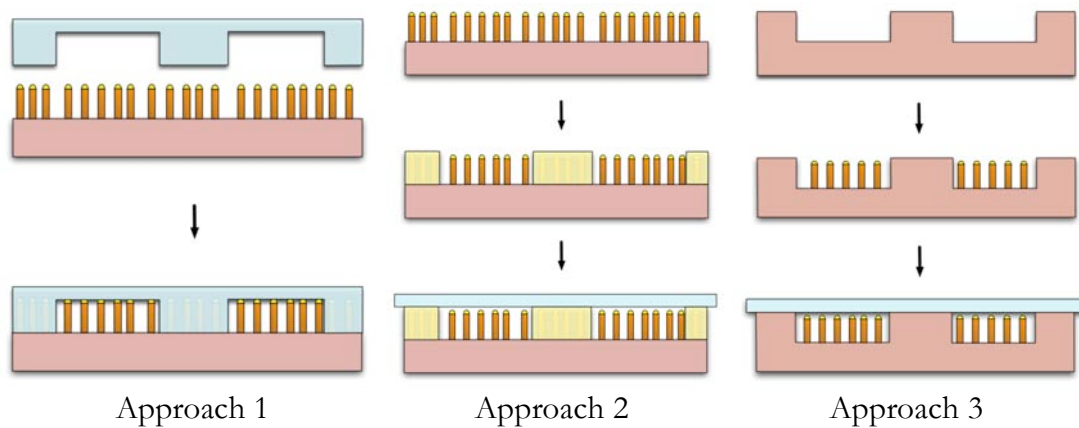
Studying nanowires in fluids will also give us more insight into the properties of nanowires such as adsorption coefficients and how nanowires withstand flows of different kind. Further, we will grow nanowires on different surfaces and in channels, which will give more insight into the growth process of nanowires.

1.2 Three ideas of channel structures around nanowires

It is essential that we are able to control the flow. A natural way of directing a fluid is to restrain its allowed paths with floor, walls and ceiling. In other words, we want to flow our aqueous solutions in sealed channels and in this project three approaches are considered:

1. Bond a substrate with trenches to a flat substrate with nanowires
2. Fabricate trenches on a substrate with nanowires and bond to a flat substrate.
3. Grow nanowires in etched trenches and bond to a flat substrate.

Advantages and drawbacks of these approaches are described in chapter three in their respective sections.



2. Theory

2.1 Microfluidics

2.1.1 Introduction

We will first discuss general fluid dynamics with most derivations kept in appendix B and then decrease the dimensions to small laminar flows. Properties of flows in channels are thereafter investigated because those are of specific interest for this project.

2.1.2 Fluids and the Navier-Stokes equations

Gases and liquids are both fluids and can be thought of as an enormous number of small rigid bodies closely packed together. All these imaginable elements are movable with respect to each other and the substance constantly deforms whenever expressed to shear stresses. Unlike a gas, a liquid is often incompressible; so we will, after a general discussion, simplify the equations to incompressible flows.

The interactions in a fluid can be described as a many-body problem with one set of equations for every tiny element and together these equations form a huge system of equations. As already the three-body problem is analytically unsolvable, so is the system for a fluid with exceptions for cases when certain simplifications can be made. Simulations are therefore very important for our understanding of fluid behaviour. A differential description of a fluid is derived in appendix B and is represented by the *Navier-Stokes equations*, B-17:

$$\rho \frac{Dv_i}{Dt} = \rho g_i - \frac{\partial P}{\partial i} + \frac{\partial}{\partial i} \left(\frac{2}{3} \mu \nabla \mathbf{v} \right) + \nabla \cdot \left(\mu \frac{\partial \mathbf{v}}{\partial i} \right) + \nabla \cdot (\mu \nabla v_i), \quad i = x, y, z$$

where \mathbf{v} is velocity, g_x is the x -component of the gravitational acceleration, μ is the viscosity and ρ is the density of the fluid.

The flows we are interested in are incompressible, which according to appendix B means $\nabla \mathbf{v} = 0$. Gravitation can be neglected for the pressures we are interested in and the Navier-Stokes equations for a small incompressible flow reduces to:

$$\rho \frac{D\mathbf{v}}{Dt} = \mu \nabla^2 \mathbf{v} - \nabla \mathbf{P}$$

The result is basically Newton's second law of motion for fluids and the equations are derived from $\sum \mathbf{F} = m\mathbf{a}$.

2.1.3 Turbulent and Laminar flows

Large fluids are often *turbulent* and behave chaotically, where an infinitesimal change in initial conditions totally change the flow pattern. The behaviour is deterministic and can be simulated and it should be possible to create Hamiltonian systems with chaotic seas and also non-Hamiltonian systems with attractors. Our weather system is an excellent example of a turbulent fluidic system and can be accurately simulated for short periods of time, but on a larger time scale the flow pattern cannot be determined even with the most accurate initial conditions. Possibly, there are also weather conditions forming chaotic seas and also states with periodic behaviour.

When scaling down in size, inertial energies decrease more rapidly than viscous energies. Viscosity thus dominates and the flow can be divided into streamlines, which slide smoothly over one another. A small bead will follow a streamline and mixing occurs only on a molecular level by diffusion. This type of flow is called *laminar* and is the most commonly encountered in microfluidic devices. [8]

To specify if a flow is laminar or turbulent, the dimensionless *Reynold's number* Re is used:

$$Re = \frac{\text{inertial forces}}{\text{viscous forces}} = \frac{D\rho v_{avg}}{\mu}, \text{ where } D \text{ is the channel diameter.}$$

$Re \ll 500$ assures a laminar flow and for $Re \gg 2000$ the flow is turbulent.

If we downscale further and investigate atomistic flows, fluctuations become palpable and, for example, Monte Carlo methods considering Boltzmann probabilities can be used to simulate flow patterns.

2.1.4 Pressure driven flows in small channels

The discussion of sizes of flows indicates that the fluids somehow are confined. Usually, the confinements are channels of varying dimensions. The degrees of freedom of the system are thereby decreased and additional properties can be

determined analytically. The Navier-Stokes equations (B-17) applied to incompressible liquids in channels give us the flow rates and flow profiles.

Resistance between walls in a channel and the fluid leads to a parabolic flow profile where the velocity is zero by the walls. [9]

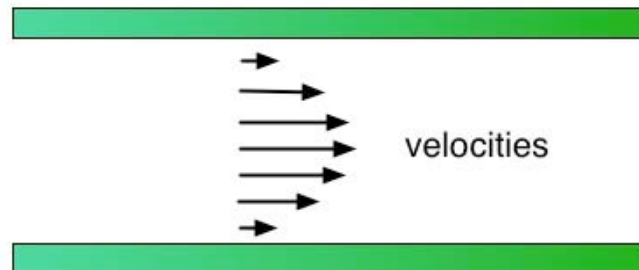


Figure 2.1: The arrows show the velocities forming a parabolic flow profile in a channel.

The flow rate Q due to a pressure drop Δp in a channel is:

$$Q = \frac{\Delta p}{R}, \text{ where } R \text{ is the resistance in the channel}$$

Note the analogy to electric circuits:

$$I = \frac{\Delta U}{R}, \text{ where } I \text{ is the current and } U \text{ is the voltage difference over the resistance } R$$

The total flow resistance R of a rectangular channel can be shown to be:

$$R = \frac{12\mu L}{wh^3} \left[1 - \frac{h}{w} \left(\frac{192}{\pi^5} \sum_{\text{odd numbers}} \tanh\left(\frac{n\pi w}{2h}\right) \right) \right]^{-1}, \text{ where } w \text{ is the width, } h \text{ height and } L \text{ is the length of the channel.}$$

The equation above is the resistance for channels with aspect ratios close to one and if the $w \gg h$ the resistance can be approximated to:

$$R = \frac{12\mu L}{wh^3}$$

It is convenient to discuss circular channels when looking at proportionalities and they have a resistance R [10]:

$$R = \frac{8\mu L}{\pi r^4}, \text{ where } r \text{ is the radius of the channel}$$

The flow rate thus decreases rapidly with decreasing dimensions of a channel as $Q \propto r^4$ and $Q \propto wh^3$. The result seems natural since the surface causes the resistance and the surface to volume ratio increases with decreasing channels. An example from real life is the rapidly decreased flow rate of your blood when your blood-vessles become thinner. The length of the channel decreases pressure gradient and thus the flow rate and viscosity is also a limiting factor. The average velocity in a channel, v_{avg} , is flow rate divided by cross sectional area:

$$v_{avg} = \frac{Q}{A} \propto h^2, r^2$$

Note that, in practice, only the smallest dimension in a channel determines the velocity, whereas both dimensions determine the flow rate. It is also important to remember that these proportionalities discussed assume a constant cross section. If the cross section suddenly increases, the same volume must come through and the velocity instead increases. To overcome the resistance in the smaller part of a channel, the pressure increases greatly, which could be a practical problem in microfluidic devices.

Consider the analogy $I = \frac{\Delta U}{R}$ again: if the molecules or particles you are interested in are charged, you can use an electric field to get a current through the device. The flow profile becomes planar and the velocity is no longer dependent on the dimensions of the channel. This process of driving a flow is called electrophoresis and is widely used in microfluidics.

Another common driving force is electroosmosis, which also gives a flat velocity profile and the possibility to drive fast flows through small channels.

2.1.5 Capillary driven flows

In this project, all flows have been capillary and this kind of driving force will now be explained. If the pressure drop that drives a fluid would increase with decreasing dimensions of a channel, this would somewhat improve the ability to drive a flow in a small channel with high resistance. For simplicity, all channels are assumed to be circular. The wetting in a channel combined with surface tension of the meniscus of a fluid gives a pressure drop over the meniscus and a net force in the forward direction as:

$$\Delta p = \frac{2\gamma \cos a}{r}, \text{ where } \gamma \text{ is the surface tension, } a \text{ the angle shown in figure 2.2}$$

and r is the radius of the channel.

Still, both velocity and flow rate increases with increasing channels, but not as much as for constant pressure. The flow rate for a tube with radius r is now:

$$Q = \frac{\Delta p}{R} = \frac{2\gamma \cos a}{r} \cdot \frac{\pi r^4}{8\mu L(t)} = \frac{\gamma \pi r^3 \cos a}{4\mu L(t)}$$

$L(t)$ is the time dependent length of the incoming flow in the channel. The pressure gradient thus decreases with time and so does the average velocity, which becomes:

$$v_{avg} = \frac{Q}{A} = \frac{\gamma r \cos a}{4\mu L(t)}$$

For capillary driven flows we thus have $v_{avg} \propto r$, instead of $v_{avg} \propto r^2$ as for normal pressure driven flows.

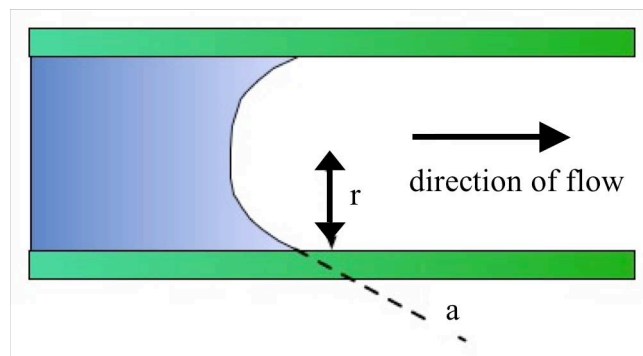


Figure 2.2: An incoming flow with its meniscus in a channel.

2.2 Nanowires

Nanowires are rod-shaped objects with two dimensions in the nanometer range. They are very much like a short strand of hair scaled down a couple of thousand times. In a nanowire thinner than the fermi length of its own material, the conducting electrons are only allowed to move along the wire. These nanowires can be considered electronically one-dimensional and their unique properties have already been used in applications. [4, 11]

New types of nanostructures and improved control over other properties of the nanowires (discussed more in the introduction) will most probable lead to several useful applications in various fields.

In principal, nanowires can be fabricated using conventional lithography techniques

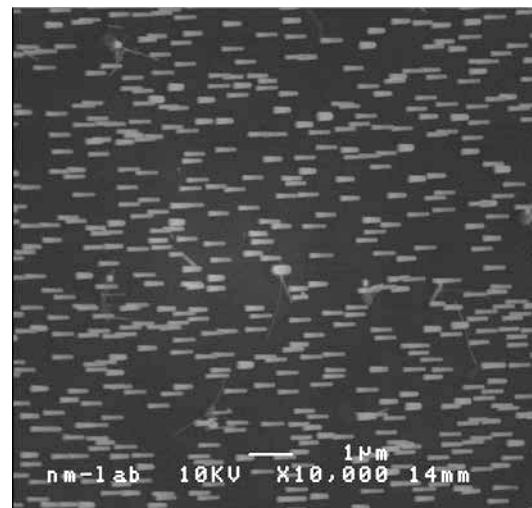


Figure 2.3: A SEM image of GaP nanowires grown on a GaP (111)B substrate. Magnification is 10kX and the sample holder was tilted 30°, grown on GaP.

or other top down methods. However, in this project only epitaxially grown nanowires are used and only those will be discussed.

2.2.1 Epitaxy

Epitaxy is a method where solid crystals are grown on top of a crystalline substrate. Material is transported to the sample either in vapour phase or in liquid phase. In vapour phase epitaxy (VPE), which was used in this project, growth material in vapour phase is flown over the sample. Atoms or molecules adsorb to the surface and bind where it is most energetically favourable, i.e. to as many atoms or molecules as possible; in crotches and steps rather than on a flat area. Therefore, each layer is finished before the next starts to grow as shown in figure 2.4 below. However, there are also other types of growth modes and this description is a simplified version of the reality. [12, 13]

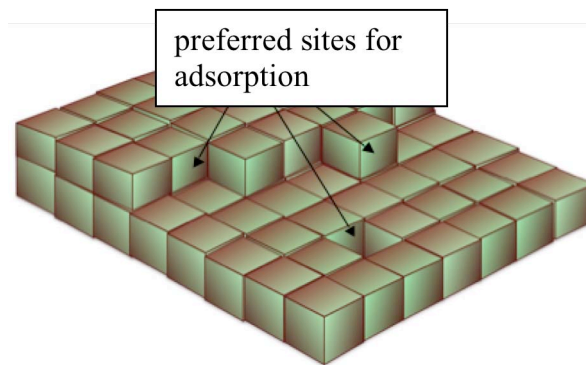


Figure 2.4: A Kossel diagram, which describes where adsorption will take place.

If there are boundaries where it becomes energetically favoured to start growing a new layer instead of continuing in the x/y -plane, the area of each layer becomes restricted and three-dimensional crystalline structures such as nanowires can be grown. In our case, these boundaries are gold particles under which the growth is preferred.

2.2.2 MOVPE-Metal-Organic Vapour Phase Epitaxy

MOVPE is a common method for growing semiconductor III-V-nanowires. The sample is placed on a graphite plate in a chamber. A radio frequency generator (RF generator) heats the graphite plate (similar to how a microwave oven heats your food) and growth material is introduced via a carrier gas, usually hydrogen (H_2). By varying temperature and gas pressures, nanowires are now grown. The vapour liquid-solid model and the vapour solid-solid model discussed below explain the processes behind nanowire growth.

When growing nanowires the growth is confined under metal particles, in our case deposited by aerosol deposition. The aerosol particles are so small that they float in air and they are directed to the substrate by an electric field. Surface coverage,

diameter and particle composition can be well controlled in this technique, but if specific patterns of nanowires are required, electron beam lithography (EBL) or nanoimprint lithography (NIL) with subsequent lift-off processes are suitable. With soft contact printing techniques specific areas with particles can be defined. [12, 14]

2.2.3 The Vapour Liquid-Solid Model

The MOVPE process can be described with the vapour liquid-solid (VLS) model, proposed by Wagner and Ellis already in the 1960's. A substrate with metal particles is heated as described above and material from the substrate is incorporated into the particles and alloys are formed. Introduced growth material in vapour phase also incorporates into the metal particles until supersaturation. The melting temperature of the alloys is lower than for the respective components (eutectic alloy) and the particles turn into liquid phase. New material will now instead form solid crystalline layers under the particles and the particles are lifted from the surface. This epitaxial growth proceeds between the particles and the newly formed layers and nanowires are created.

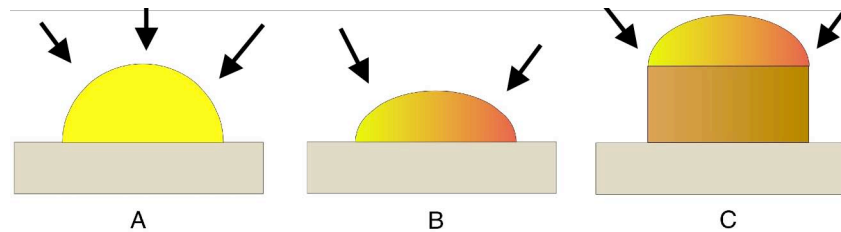


Figure 2.5: The Vapour Liquid-Solid model. (A) shows the initial metal particle, in (B) an alloy is formed and in (C) the nanowire growth has started.

As discussed above, epitaxy is an energy minimizing process and growth will be favoured in the crystal plane with lowest surface energy. In most cases this is the (111) plane. Depending on the crystal orientation of the cut substrate, nanowires will grow in different angles, i.e. (111) substrates will get nanowires perpendicular to the surface. However, after initiation of the growth, subsequent layers grow on already grown layers and are no longer dependent on the crystal orientation of the substrate. It is therefore possible to grow nanowires with material and structure different from the substrate and, with controlled initiation it is even possible to grow crystalline nanowires on non-crystalline substrates. [12, 13]

2.2.4 The Vapour Solid-Solid Model

The vapour liquid-solid model does not totally agree with experimental results. For example, nanowires have been grown at temperatures lower than the melting point for the eutectic seed particles. Kimberly Dick et al. recently presented their results that show nanowire growth only when the seed particle is supposed to be in its solid phase [15]. This result supports another model for growth of III-V nanowires proposed last year by Ann Persson et al. They call it *Solid-phase diffusion mechanism* and

it is based on a solid seed particle. Under the particle, the surface energy is lower than for the surroundings and growth will therefore be favoured there. Only the III component incorporates in the metal particle and will, after dissolution, diffuse through the particle. In the interface between the seed particle and the nanowire, the III-component reacts with the V-component to form a crystalline III-V layer. The V-component is probably incorporated directly into the interface. [16]

2.3 FABRICATION

In this section all fabrication techniques are discussed. Basic theory is explained; recipes and detailed procedures are described in appendix A.

2.3.1 Bonding by Oxygen ashing

In this project, oxygen plasma ashing was used for preparing surfaces for bonding. The samples are placed in a vacuum chamber and oxygen is introduced. Microwaves (we actually use a conventional microwave oven that has been re-built) dissociate the oxygen molecules to single atoms that react with the surfaces of the samples.

Exposed to plasma ashing, silicon based material with Si-CH₃-groups react to form Si-OH-groups (silanol groups) on the surface. When pressed together silanol groups naturally form Si-O-Si plus water in a condensation reaction. Silicon based materials can therefore be covalently bonded together after oxygen plasma treatment. Further, the hydroxyl part in the silanol group makes the surfaces hydrophilic and wetting with hydrophilic biological samples is facilitated. Diffusion of molecules inside a sample makes the hydrophilicity temporary and after less than hours, the molecules have diffused to the surface, which becomes hydrophobic again.

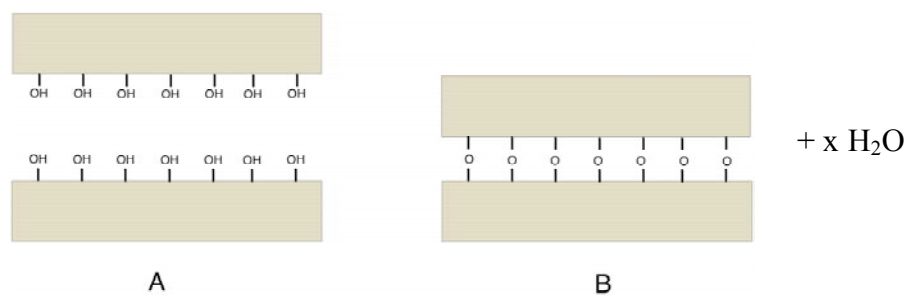


Figure 2.6: (A) Hydroxyl groups are formed after oxygen ashing and (B) the wafers bond covalently to each other. The rest product is water.

2.3.3 UV-lithography

Photolithography is a conventional method used for making structures on top of a substrate, for example to be used as etching mask. The method is quick, easy to use and produce nice structures down to micrometer sizes. ¹

A substrate is coated with a UV-light sensitive photo resist by spin coating, during which the sample is rotated rapidly and photo resist deposited is spread due to lack of centripetal forces to form a homogenous thin layer on top of the sample substrate. The thickness of the film is determined by the speed of rotation, which is easily varied and optimised for the specific purpose.

UV-light is then shone on the sample through a mask and exposed photo resist is damaged or cross-linked and stabilized depending on whether it is a positive or negative photo resist (see figure 2.6). The mask is usually made of a glass slide covered with chrome that has been selectively patterned with a large specialized laser writer to form the preferred pattern. After exposure, damaged resist (or not cross-linked resist) is removed in the development process and the pattern of the chrome mask is transferred to the photo resist layer. [17]

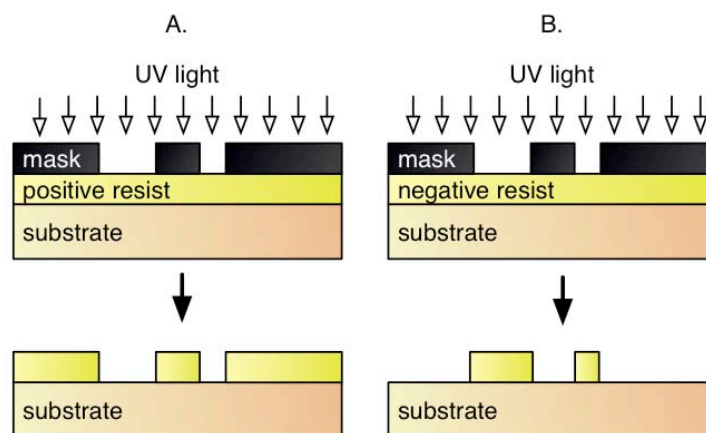


Figure 2.6: This scheme describes the lithography result for (A) positive and (B) negative resists respectively.

2.3.4 Plasma Enhanced Chemical Vapour Deposition (PECVD)

PECVD is used for creating thin films of material on a substrate. The method is similar to MOVPE discussed above, which actually also is denoted MOCVD (Metal-

¹ The word “lithography” comes from the two greek words $\lambda\iota\theta\omicron\varsigma$ (lithos) and $\gamma\rho\alpha\varphi\omega$ (gráphein) and basically means “to write in stone”, which Aloys Senefelder did in the 18th century.

Organic Chemical Vapour Deposition), but no carrier gas is used and the deposition is driven by a plasma.

Gases are fed into a vacuum chamber in which the sample is placed. An RF-generator dissociates the gases into radicals and makes them reactive so that they will adsorb to the substrate surface via chemical reactions and form a thin homogenous layer. A great advantage for PECVD is that the operating temperature is much lower than for conventional chemical vapour deposition (CVD) in which very high temperatures are needed in order for the gases to become reactive. Still, hundreds of degrees celsius are required in PECVD to get a film with high surface density and good quality and this must be considered when developing our methods. [18]

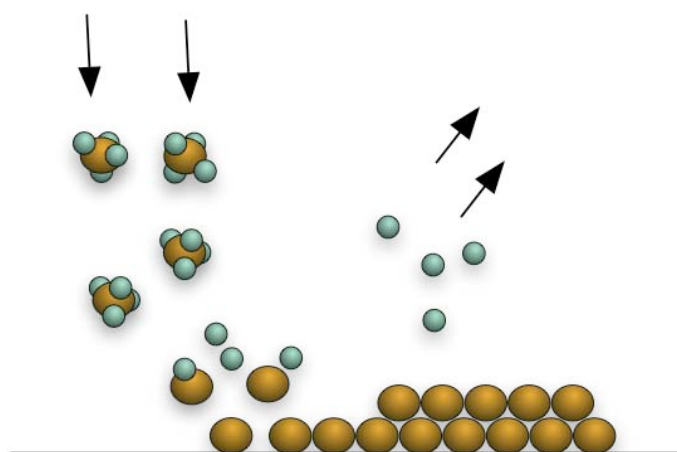


Figure 2.7: Schematic illustration of how a crystalline film is formed by PECVD. Note that in the illustration only one gas is dissociated, in reality usually two or more gases are used to form for example silicon nitride on the surface.

2.3.5 Thermal Evaporation of Silicon Oxide

Unlike various CVD techniques, in thermal evaporation the sample is not heated significantly and this is the greatest advantage of this method of creating thin films on a substrate. Unfortunately, the film quality is not as good as for CVD, but evaporated silicon oxide layers should be good enough to provide bonding to PDMS after oxygen plasma ashing.

The sample is mounted on a sample holder and placed upside down in a vacuum chamber. Silicon mono oxide (SiO) resides in a “boat” made of Tungsten. A current heats the boat and the SiO to hundreds of degrees celsius until the SiO sublimates (material in gas phase leaves the solid material). The sublimated gas has a long mean free path due to the vacuum and easily reaches the sample where it is de-sublimated and a thin film is formed. The thickness of the film is measured with an oscillating quartz crystal, whose resonance frequency decreases with deposited material.

2.3.6 Reactive ion etching (RIE)

This anisotropic etching method is excellent for etching trenches on a substrate if one has a suitable etching mask. The sample is put into a vacuum chamber and gases are introduced. These gases are dissociated by an RF-generator and at the same time accelerated towards the sample surface. This leads to formation of dangling bonds and dislocations in the substrate, which in turn becomes reactive to the etchant. Molecules on the surface react with the decomposed gases and produce new molecules in gas phase. These new gases are pumped away and material has been etched away.

The energy driven bombardment produces an anisotropic etch and allows us to reduce undercut. The anisotropy is maximized with a long mean free path for the molecules, realized with high acceleration and low pressure. [17]

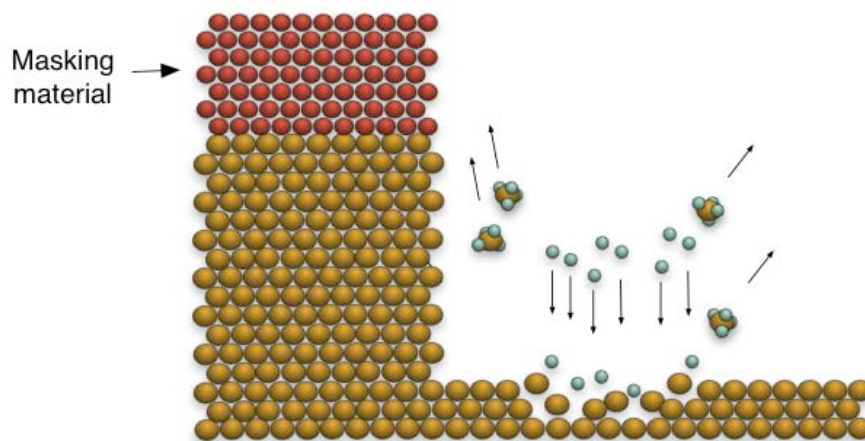


Figure 2.8: Illustration of the RIE method when an etching mask is used. Dissociated etching molecules are accelerated towards the substrate, which causes dangling bonds. New molecules are formed and are pumped away from the sample.

2.3.7 Wet etching

As the name implies, your whole sample is placed in a liquid etching solution during wet etching. Material is removed chemically when molecules on the substrate react with etchant molecules.

Isotropic wet etching is good for removing surface damage and polish substrates, but if we want to etch trenches with smooth surface using an etching mask it is preferred to etch anisotropically. Fortunately, there are anisotropic wet etching methods, where the etching rate is higher for certain crystallographic orientations of the substrate. Profiles and results from wet etching will be discussed in Ch4. [17, 19]

2.3.8 PDMS molding

Poly(dimethylsiloxane) (PDMS) is widely used in MEMS applications because it is easy to use, bio compatible, less expensive than many other materials and optically transparent down to 230nm. Further it can be bonded to Silicon based materials after oxygen ashing. PDMS is composed of two components, that when mixed and baked (45min in 80°C) become a solid silicon rubber. Therefore, 3D structures can be molded in a form and cured. The form, usually called master, was in our case a silicon wafer etched with RIE after UV-lithography. To avoid the PDMS sticking to the master, the master is coated with fluoro-silane. [20]

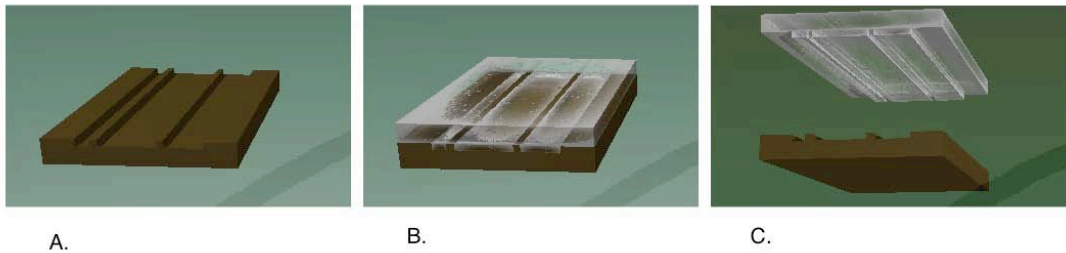


Figure 2.9: Scheme for soft lithography of 3D PDMS structures. First the empty master (A), then PDMS is poured into the form (B) and after curing the PDMS sheet is peeled of (C).

2.4 IMAGING TECHNIQUES

We want to image our results from lithography, etching, nanowire growth etc. High-resolution techniques are needed in order to resolve the interesting nanometer details. Atomic Force Microscopy (AFM) and Scanning Electron Microscopy (SEM) are two convenient tools that complement each other well.

Another type of imaging is needed to record the flow of DNA through our channels. For this, epifluorescence microscopy is used.

2.4.1 Atomic Force Microscopy

The force between neutral atoms can be described with the negative derivative of the Lennard Jones-potential:

$$F = 24\epsilon \left(\frac{2\sigma^{12}}{z^{13}} - \frac{\sigma^6}{z^7} \right), \text{ where } \sigma \text{ and } \epsilon \text{ are material constants and } z \text{ is the distance}$$

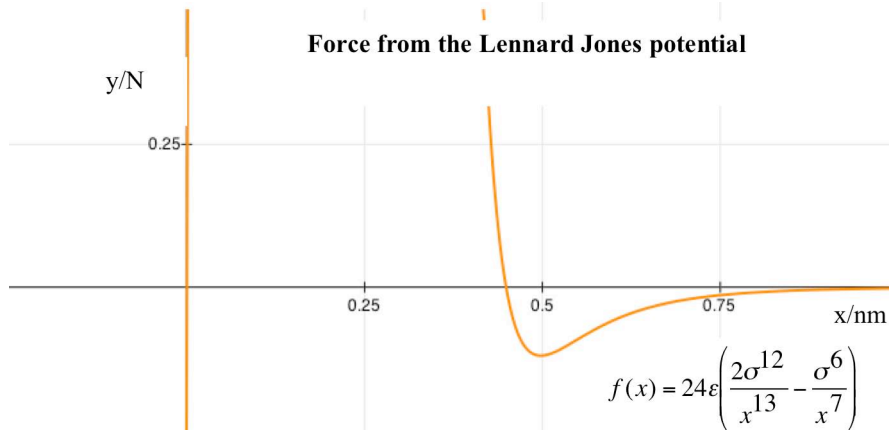


Figure 2.10: The force curve between two neutral atoms represented by the derivative of the Lennard Jones potential for $\epsilon=0.02\text{eV}$ and $\sigma=0.4\text{nm}$.

This force depends on distance and that property is used in an AFM. A cantilever with a small tip is placed over the sample and scans the sample using a piezoelectric movement system. Somewhat simplified, the deflection of the cantilever resembles the topography of the sample and is detected using a laser beam and a photo detector as shown in figure 2.11.

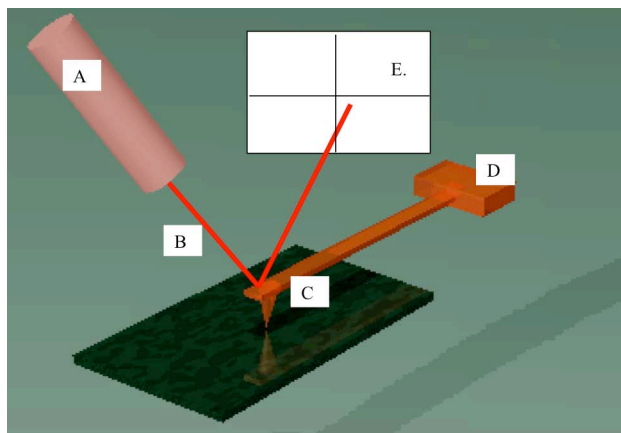


Figure 2.11: A typical AFM setup. The laser (A) emits a beam (B), which reflects on the cantilever (C) and is detected on a photo detector (E).

Contact mode AFM is very common and uses the repulsive region of the force curve. The cantilever scans the sample, which topography is, either by using a feedback loop to keep the force and thus the distance between cantilever and sample constant, or by measuring how the force on the cantilever changes when scanning.

In this project we will mostly use *tapping mode AFM*, which is less harmful to the sample. The cantilever tip is oscillating at its resonance frequency and is only in

contact with the sample for short fractions of time. In this mode, additional properties apart from the Lennard-Jones potential are used to image the sample.

If the sample is fragile and with high aspect ratio features, it might be interesting to use *non-contact mode AFM*, where the cantilever is oscillating at its resonance frequency further away from the sample, where the force is attractive. [12, 21]

It should also be mentioned that there are other types of scanning probe microscopes (SPM) than AFM. Magnetic Force Microscopy (MFM) is one example where the magnetic force is used to image magnetic topology.

2.4.2 Scanning Electron Microscopy

It is the relatively long wavelength of visible light that limits the spatial resolution in an optical microscope. Electrons have a much shorter de Broglie wavelength and the possible resolution in an electron microscope is correspondingly higher. Features down to about one nanometer can be resolved, however it is not the diffraction limit, but lens aberrations that sets the limit.

Scanning Electron Microscope (SEM) is a common system and a technique that has been used in this project. In a SEM, an electron gun emits electrons, which are accelerated (around 10kV) and focused by metal apertures and magnetic lenses to interact with the sample at a small area. The interaction leads to scattered primary electrons, emitted secondary electrons, x-rays etc. They all contain information about the sample so that topography, material properties etc can be determined. As the name suggests, the electron beam scans over the sample to capture an image, which is shown on a computer screen. The electron gun is not moving, the beam is instead directed electro-magnetically. The whole procedure is done under vacuum to provide a long enough mean free path for the electrons. [12, 22, 23]

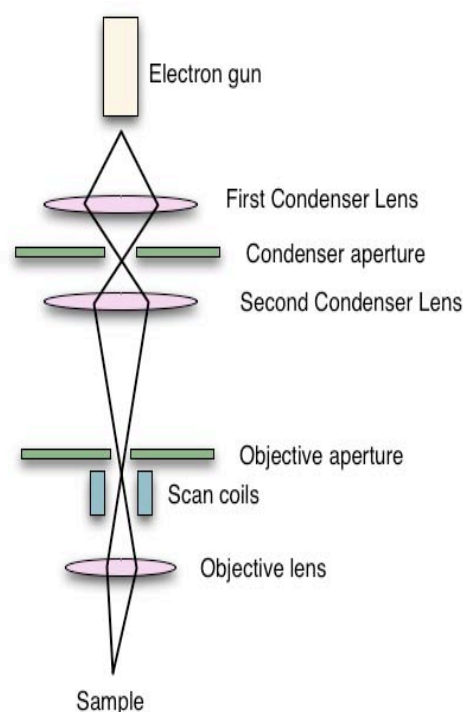


Figure 2.12: The path of the electrons in a scanning electron microscope

2.4.3 Epifluorescence Microscopy

Fluorescent DNA flowing in a microfluidic device can be imaged and recorded with an epifluorescent microscope setup. Epifluorescent microscopes are useful whenever fluorescing molecules in the sample are of interest. The diffraction limit of visible

light limits the resolution in normal optical microscopes. Resolution is not changed in an epifluorescence microscope, however, the positions of small fluorescing molecules can from multiple measurements be determined within a few nanometers.

A UV-lamp (or another light source that can excite molecules in the sample) sends light that is collimated and directed into an excitation filter so that everything but the wavelengths that excite the sample is blocked. A dichroic mirror reflects the excitation light, which travels through an objective to the sample. Molecules in the sample are excited and emit light, usually isotropically. The emitted light that goes back through the objective is not reflected, but transmitted by the dichroic mirror. An emission filter further filters out non-emission wavelengths and the light can finally be detected using a charge coupled device camera (CCD camera) or by looking through an ocular. The CCD camera's images can be recorded in real-time and movies of for example flowing DNA can be acquired. [24]

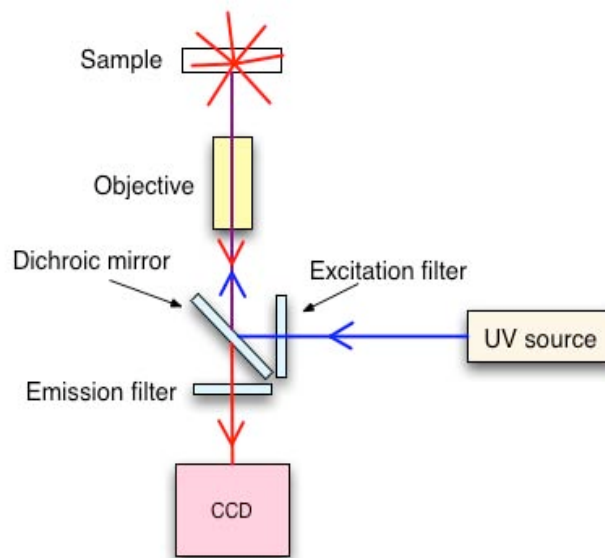


Figure 2.13: The setup of an epifluorescence microscope. The excitation light is collimated and goes through an excitation filter. The dichroic mirror reflects the beam which goes through the objective and excites molecules in the sample. The emitted light travels back through the objective, the dichroic mirror and an emission filter. A CCD camera or similar detects the emitted light.

3. General bonding experiments

Bonding turned out to be a critical step in all methods. Therefore, many experiments without nanowires were performed to learn which materials can be bonded together and how the bonding is optimised.

3.1 Oxygen plasma bonding

Introduction

In order to develop the different methods it was important to investigate which materials could be bonded to each other. For this project it was critical that the bonding would provide sealed undamaged channels for DNA flows. However, every sample with channels takes time to produce and hence, bonding tests with flat devices were first performed.

Method

New methods and ideas, often concerning new materials, were discussed all the way through the project and subsequent bonding experiments were carried out. With gained knowledge about bonding, it was easier to determine if a method was realizable. During the project, we tested bonding after 30-75s of oxygen plasma, of PDMS to several materials. The test material was placed in the plasma ashing machine together with one piece of PDMS for bonding and two extra pieces of PDMS for testing the quality of the PDMS and the ashing by bonding PDMS to PDMS. The bonding strength was then tested with vacuum tweezers or by pulling and pushing with conventional tweezers.

The following materials were tested: PDMS, silicon, glass, gallium phosphide, SU8 (a negative photo resist), silicon nitride (PECVD), spin on glass (SOG) and silicon oxide (thermally evaporated).

Results

Table 1: Results from oxygen ashing and bonding to PDMS for a number of different materials.

Material	Bonds to PDMS
PDMS	Yes
Silicon	Yes
Glass	Yes
Gallium Phosphide	No
SU-8	No
Silicon nitride (PECVD)	Yes
SOG	Yes
Silicon oxide (thermal)	Yes

Discussion and conclusion

It must first be said that the results varied greatly even for the same materials and occasionally, even PDMS to PDMS failed to bond. Therefore, something apart from choice of material must also be central when bonding after oxygen plasma. Varying the time of ashing between 30 and 60 s did not affect the results and neither did the age of the cured PDMS. Cleaning of the PDMS in ethanol under sonication tended to provide better bonding, however some tests with non-cleaned PDMS were more successful than other tests with cleaned PDMS.

Whenever PDMS successfully bonded to itself, the test result could be considered reliable and led to the table above, which now can be used when choosing materials for different methods. However it is of importance to optimise the oxygen bonding procedure not to unnecessarily ruin any samples.

GaP and SU8 failed to bond to PDMS because no hydroxyl groups (-OH) are formed on the surface during oxygen ashing. The covalent bonding is therefore not possible. On the other hand, all other materials tested contain silicon and Si-OH groups are formed and provide bonding.

3.2 Bonding in NIL machine

Introduction and method

One approach of integrating nanowires with microfluidics is to fabricate channels around nanowires standing on a substrate (see section 4-introduction and 4.2). Lithography of channels with a permanent photoresist, such as the epoxy based SU-8, is suitable. Billenberg et al describe how to bond SU-8 to poly-methylmethacrylate (PMMA) in [25]. In short words (recipe in Appendix A), PMMA 950k a5 is spin coated onto a glass substrate, soft baked and placed, with PMMA facing down, on a

substrate with SU-8 channels. The sealing is finalized by pressing and heating in a nanoimprint machine. The channels are $10\mu\text{m}$ wide and $2\mu\text{m}$ deep.

In contrast to the bonding tests with oxygen plasma, samples with channels were used from the beginning because samples with channels do not take much longer time to produce than samples with plain SU-8. The channels were first examined in an optical microscope, then the bonding was tested with vacuum tweezers and last, the sealed channels were tested by flowing DNA through them using the method described in section 4.0-*Experimental setup for flowing DNA in channels*.

Result - The edge bead problem

Pressure and temperature are two important parameters when optimizing bonding with this method, however other issues turned out to be even more critical for any bonding at all to take place. It is important that both surfaces are flat and *the edge bead* could therefore be a problem. Lack of centripetal forces during spin coating drive the resist from the sample and surface energy keeps some resist from falling off. The equilibrium between these forces determines the thickness of the spin-coated film. By the edges, it is more difficult for the resist to move further out on the sample and therefore a wall of resist is created around the sample. The edge bead was a problem in three different ways:

1. During exposure in the contact aligner the edge bead prevents a proper contact between the mask and the sample resulting in clogging around the edges. This effect was almost totally prevented by optimizing different lithography parameters.
2. When pressing the SU-8 against the PMMA, the high edges got more pressure and the channels collapsed and got clogged. This would prevent a liquid from flowing through the device. (figure 3.1)

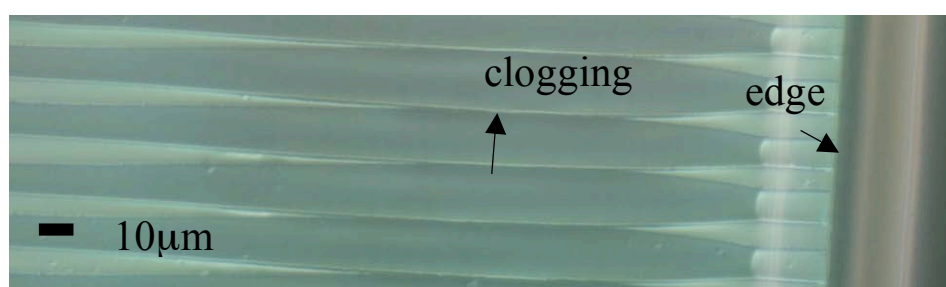


Figure 3.1: Optical image showing how the SU-8 channels close to edges are pressed together and clogged because of the edge bead.

3. The edge bead prevents inner parts of the surfaces to get into contact and bond properly.

Various ways of avoiding the edge bead were investigated. Edge bead remover was not an alternative, because the samples were very small and not circular. If the structures by the edges are important to keep, one can use PDMS instead of glass as supporting material for the PMMA (figure 3.2). The pressure during bonding will

then even out better throughout the samples. This method however was not totally straight forward and the bonding parameters must be optimised to compensate for the soft PDMS taking up more of the pressure than glass does.

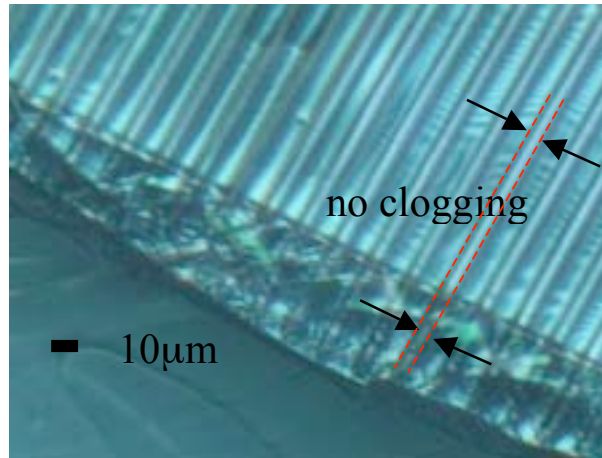


Figure 3.2: Optical image of SU-8 bonded to PMMA supported by a plain piece of PDMS. Although the edge bead was not removed, there was still no clogging of the inlets and outlets of the channels

We found the best way of removing the edge bead to be to simply *scratch the edges* with a scalpel after soft bake. The whole surface then becomes flat and bonding is more likely to be successful. If big devices are available one can also cut out a flat piece after the lithography process and still get channels close to the edges.

Result – Bonding

Several experiments with devices from successful bonding tests show non-stretched DNA flowing in channels. The DNA did not seem to stick to the channels and surface modifications are therefore not necessary. There were always non-bonded areas where DNA was moving across the channels ($\approx 50\%$ bonding). Increasing the pressure did not improve the bonding and too high pressure deformed some of the channels. Raising temperature from 110°C to 120°C in the bonding process seemed to worsen the bonding quality. Important to note is that the bonding became worse during the experiments; tight areas suddenly had DNA all over.

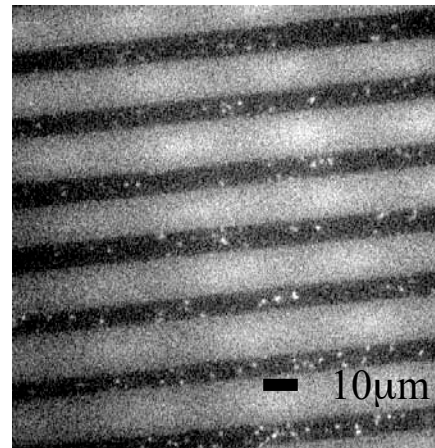


Figure 3.3: Non-stretched DNA flowing in channels.

Discussion and conclusion

The method is promising and although it needs improvements, we can use samples with SU8 channels containing nanowires in further experiments. Hopefully, improved bonding will also prevent the bonding from deteriorating during the experiments. The SU8 channels are often not perfectly flat, which could be one reason why there is

not bonding everywhere. A possible solution is to use Su8 instead of PMMA as the other bonding layer, because SU8 has a lower viscosity. However the lower viscosity could also lead to clogging of the channels. Of imaging reasons, SU8 is not preferred because it fluoresces.

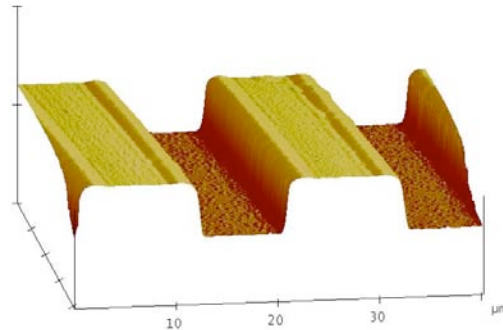


Figure 3.4: An AFM image of SU8 channels, 10 μm wide and 2 μm deep. It shows that the surface is not flat and this could prevent bonding.

DNA flowing in channels, with nanowires as obstacles, should be stretched out whenever they stick to a nanowire. For comparison reasons it was therefore positive that the DNA did not stretch in these experiments.

4. Integrating Nanowires and Microfluidics

4.0 Experimental setup for flowing DNA in channels

This setup was used in all three approaches of integrating nanowires with microfluidics. The wafer was bonded to glass or PDMS depending on method and glued or taped to two pieces of a cut object glass to fit in the chuck of the epifluorescence microscope. A 5 μ l drop of 48.5kbp long (16 μ m) TOTO-1 stained λ -DNA, 0.5 μ g/ μ l in $\frac{1}{2}$ TB buffer was placed on one side of the wafer. The fluorescing flow was detected with a 60X NA 1.0 water immersion objective and recorded on a computer.

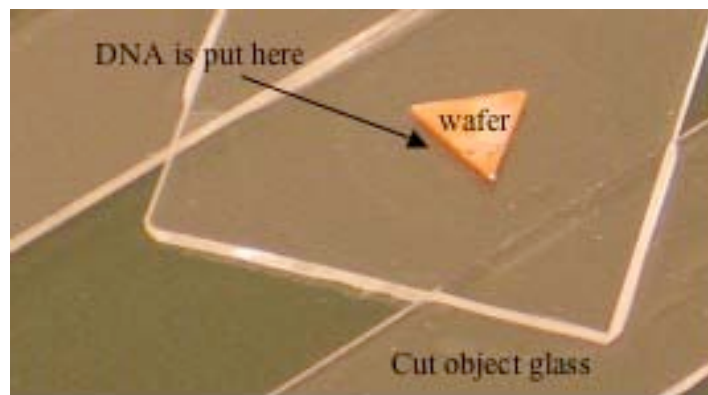


Figure 4.1: Image of a typical device.

4.1 Channels on the reciprocal substrate

Introduction and method

Not seldom, simple ideas are successful, not because nature tends to favour simple solutions, but rather because they often depend on a few well-optimized, conventional processes with fewer unfamiliar steps that can then get in the way. Possible problems can more easily be foreseen already in the planning stage of a project.

The first approach we wanted to try out was therefore to bond a wafer with grown nanowires to a PDMS sheet with predefined channels. The nanowires are then supposed to penetrate the soft PDMS to create sealed structures.

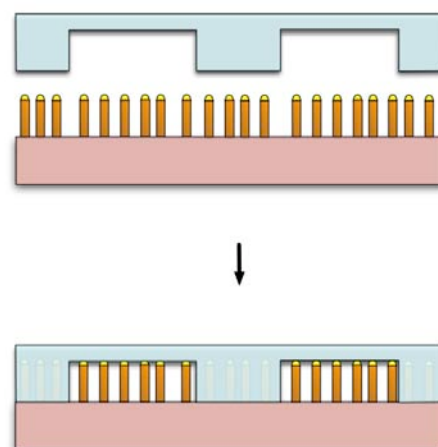


Figure 4.2: The principal of approach one.

Silicon Nitride is deposited with PECVD on a GaP wafer with straight GaP nanowires because SiN provides bonding, while GaP does not. After oxygen ashing the wafer is then bonded to a PDMS sheet with predefined channels with width $10\mu\text{m}$ and depth $1.5\mu\text{m}$. The PDMS sheet is cleaned in ethanol to get rid of un-polymerised PDMS before the bonding procedure. Flowing DNA in the channels with the setup described above tests the channels. For comparison reasons and to test the experimental setup, tests were performed using samples without nanowires.

Results

The tests with samples without nanowires were successful, with DNA flowing for a long time in the channels. Unfortunately, the bonding did not work for substrates containing nanowires and the DNA was flowing everywhere.

Discussion and conclusion

The nanowires prevented to close contact between the PDMS and the wafer and bonding was therefore not possible. This is not very surprising though oxygen bonding requires flat and clean surfaces. Some nanowires could still have penetrated the PDMS and this can probably be useful in other applications.

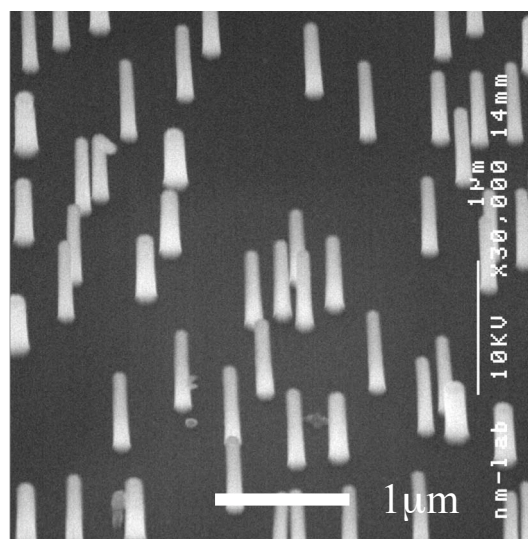


Figure 4.3: 30° tilted SEM image of GaP wires covered with silicon nitride.

4.2 Construction of channels around nanowires

Introduction

It is known that nanowires are strong and they can withstand the harsh treatment of spinning. We were then to develop a method where channels on the nanowire substrate are defined using UV-lithography and subsequently bonded to a flat substrate. Choice of material of the nanowire substrate does not affect the method and this is a great advantage.

Method

A permanent resist is preferred because the lithographed channels do not act as a mask, but as the final channels for flowing DNA. SU8 is known as a strong resist, very difficult to strip and that withstands very high temperatures. SU8 is therefore spin coated onto a GaP sample with $\approx 1.5\mu\text{m}$ long GaP nanowires. High acceleration decreases the edge bead, but edge bead scraping is still needed to provide bonding. $10\mu\text{m}$ wide and $2\mu\text{m}$ deep channels are then created according to the recipe in appendix A.

We concentrated on two different bonding procedures where one is the method tested without nanowires in section 3.2. The SU8 channels are bonded to a glass slide covered with PMMA, using a nanoimprint machine (NIL machine) with which pressure and temperatures can be controlled.

The other bonding method is to deposit 25 nm of silicon nitride in PECVD on the channels and bond to a flat piece of PDMS after oxygen ashing. SiN will cover the nanowires and since surface modifications on SiN are well developed, this is positive for many applications although the diameter of the nanowires will change. As shown in section 3, we could have used SiO_x instead of SiN to get a layer for bonding and this alternative method is still to be investigated. Our method is first tested using samples without nanowires: SU8 channels are fabricated on a plain piece of Si wafer. Silicon nitride is deposited in PECVD to provide bonding to PDMS after plasma treatment.

In both bonding approaches, flowing DNA through them as described in section 4.0 tests the channels.

Result and discussion for the lithography process

SU8 channels were successfully fabricated around the nanowires. The left image in figure 4.5 shows that “arms” of SU8 has got stuck in the channels. This could be due to a non-optimised lithography process. I think it is more likely that some SU8 is

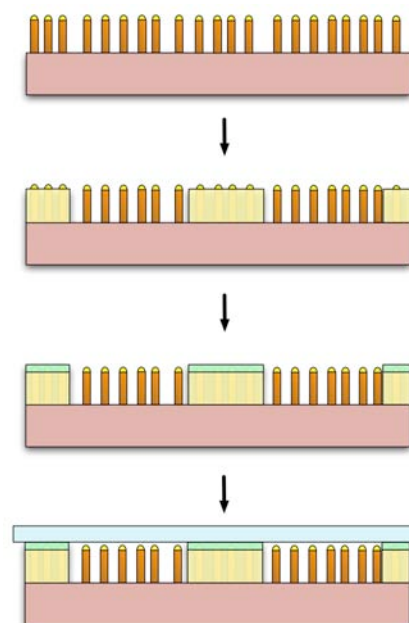


Figure 4.4: Scheme of making channels around nanowires. First, SU8 is lithographed, then SiN is deposited to provide the subsequent bonding to PDMS.

stuck around the nanowires and are therefore more difficult to rinse off in the development.

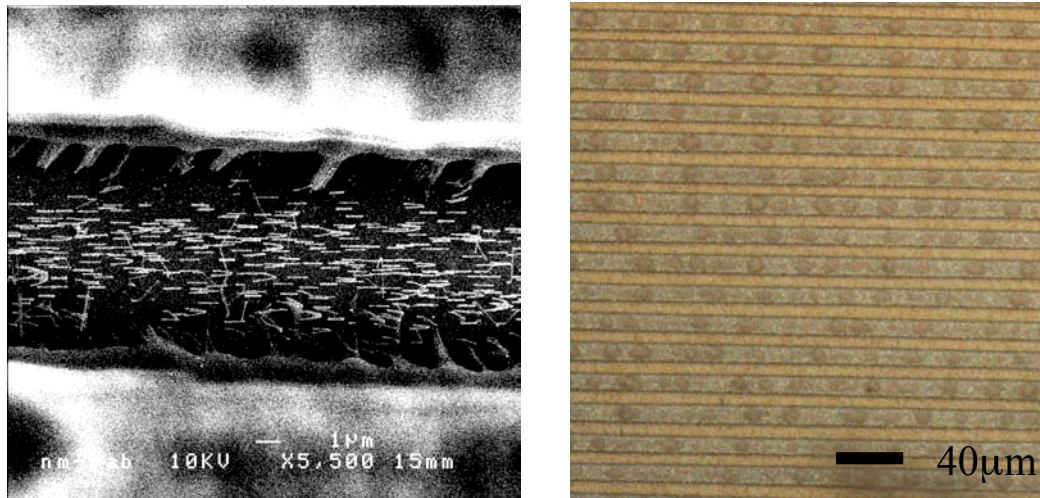


Figure 4.5: (left) SEM image showing nanowires standing in a 10 μm wide trench. (right) An optical image of SU8 channels around nanowires. Magnification is 20X and each channel is 10 μm wide.

Result and discussion for the NIL-bonding approach

DNA was successfully flown in channels and this was to my knowledge the first time a liquid was flown in channels containing straight nanowires. The acquired films show DNA stretching out around nanowires (see figure 4.6) and this proves that the nanowires easily withstand the flow and the forces from DNA bumping into them. All DNA was not stretched out because the forest of nanowires was not very dense and there was also a gap of approximately 0.5 μm between the nanowires and the ceiling in the channels.

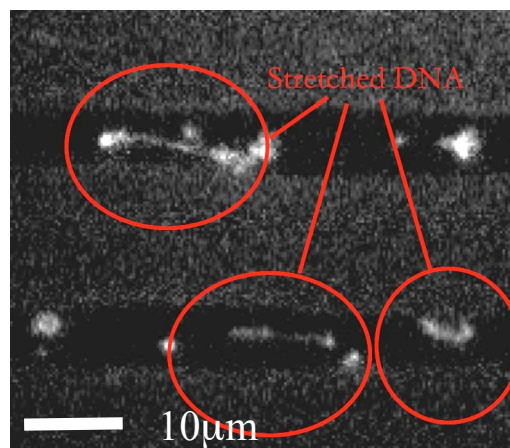


Figure 4.6: One frame from a movie of DNA flowing in channels with nanowires. The red circles mark spots with stretched DNA.

All areas where not bonded properly ($\approx 10\%$ was bonded) and the method can be further optimised. In the SEM image in figure 4.5, the surface of the SU8 does not look very flat and smooth, which naturally affects the bonding result. However, an AFM image of the device (figure 4.7) together with an AFM image of a device without nanowires (figure 3.4) shows similar flatness and thus, the poorer result for devices containing nanowires does not depend on non-flat surfaces. (Note that the nanowires cannot be correctly imaged in the AFM, which results in the rough areas inside the channels.)

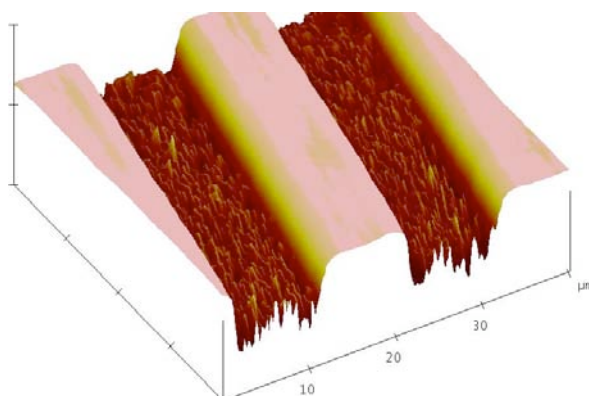


Figure 4.7: An AFM image of SU8 channels made on a substrate with nanowires.

Results and discussion for the oxygen bonding method

The SU8 channels were not affected by the high temperature (350°C) in the PECVD process. Further, the tests without nanowires were successful with non-stretched DNA flowing in the channels. Unlike the SU8/PMMA approach, the bonding did not deteriorate with time and that is promising for future applications where devices need to work for long times. Some channels, especially those with low aspect ratio, collapsed with soft PDMS sticking to the bottom of the channels.

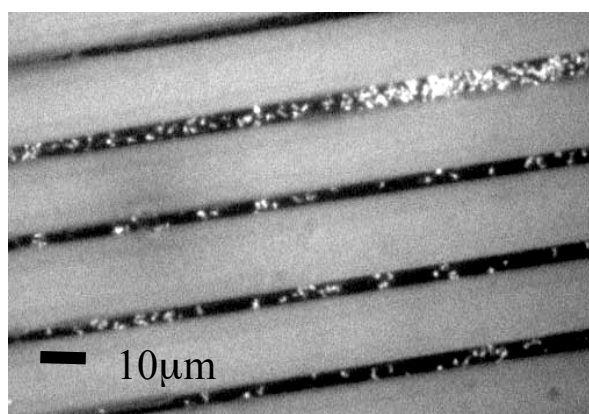


Figure 4.8: DNA flowing in SU8/SiN/PDMS channels on a sample without nanowires.

Also for samples containing nanowires we managed to get DNA flowing in the channels (figure 4.8). The DNA, however, did not seem to stretch out as it did for the SU8/PMMA bonding method. One could think that the distance between nanowires and ceiling and/or between nanowires is too large, however very similar devices were used in both methods with equally dimensioned nanowires and the same thickness of the SU8. The two bonding methods include different materials, but since DNA did not adsorb to any surfaces in either method I do not believe that this determines whether DNA stretches out or not either.

In the SiN deposition, the nanowires get slightly thicker, which should only increase the stretching, because the spacings between the nanowires decrease. A possible explanation is that the nanowires broke from soft PDMS getting down in the channels during the oxygen bonding process, however in section 4.3 we will use PDMS as bonding layer and again have DNA stretching out. The non-stretching of DNA was probably due to unknown mistakes in the experiment and we need several more experiments before any conclusions can be drawn.

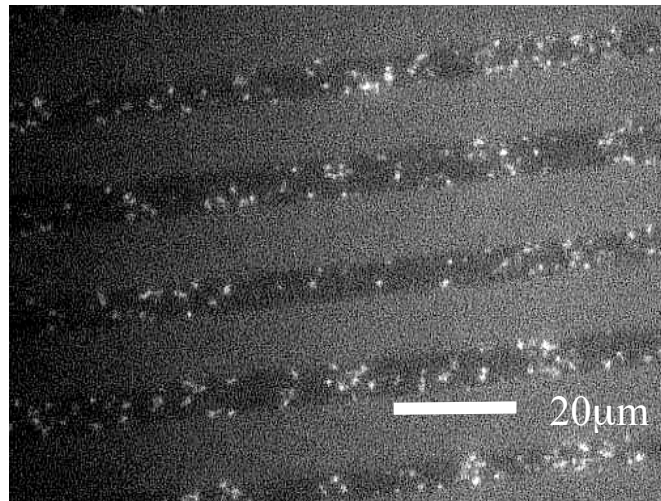


Figure 4.9: DNA flowing on a sample with GaP nanowires in channels made of SiN covered SU8 bonded to PDMS after oxygen ashing.

4.4 Growth of nanostructures in etched trenches

Even though UV-lithography is a conventional method, it contains many steps where the samples containing nanowires might be damaged and rendered useless. It would therefore be convenient to fabricate the channels before growing the nanowires. In this approach we will etch trenches in which nanowires, nanotrees and other nanostructures can be grown.

For future applications, it is important to be able to align nanowires in specific patterns in channels and this is difficult, although possible, when using lithography to produce channels around nanowires as in approach 2. With predefined trenches, alignment of patterns can be made with for example EBL. [23]

Further, the newly invented nanotrees are more fragile than normal nanowires and do not seem to withstand the spinning process. This third approach is therefore promising for integration of branched nanostructures with microfluidics. [7]

Apart from already discussed advantages, we will also gain important knowledge about nanowire growth on etched surfaces and about how nanowire growth depends on the geometry of channels.

4.4.0 Choice of materials

The crust of the Earth contains 25% silicon, which therefore is a very common material and naturally less costly compared to other semiconductor materials. On silicon, one can thermally grow silicon dioxide (SiO_2), which is a very good insulator and also often an excellent etch mask. The fact that silicon is the dominating material used in semiconductor devices makes it important to enable nanowire growth on silicon. Following integration with microfluidics is desirable for bio applications. Therefore we wanted to etch channels in Si for subsequent nanowire growth.

However, so far, compound III-V semiconductors, such as gallium phosphide (GaP) and indium phosphide (InP), have shown to be excellent supporting materials for growing nanowires in MOVPE. In addition, III-V materials have unique optical and electrical properties that are useful in various types of applications. For example GaP is nearly transparent. One part of this project was therefore to etch trenches in GaP for subsequent nanowire growth. [12]

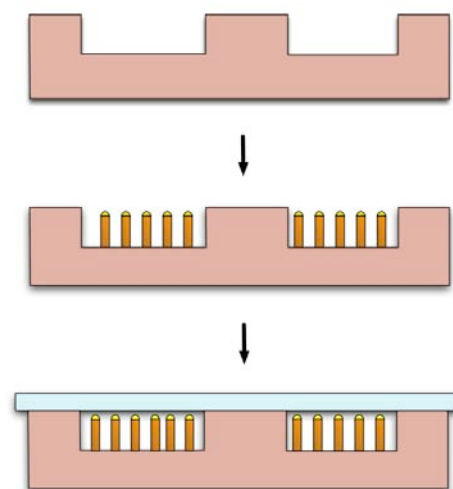


Figure 4.10: The principal of approach three.

Nanowires are not necessarily of the same material as the substrate they are grown from and nanowires have been grown in various non-III-V materials such as Si, silver (Ag), gold (Au) and combinations thereof. [2, 26, 27] In this project, GaP nanowires were grown on both GaP and on Si. The optical and electrical properties of the III-V semiconductor GaP can thus be used with silicon as substrate, an optimal solution.

4.4.1 Growing nanowires in etched gallium phosphide channels

Method

Figure 4.11 shows the procedure of growing GaP nanowires in etched GaP channels avoiding growth outside the channels. S1813 and SiN are used as etching mask for the two wet etching recipes used. The main purpose of SiN is to provide bonding to PDMS after oxygen ashing. Thermally evaporated SiO was not used, because it does not withstand the high temperatures in MOVPE during nanowire growth. We did not have the possibility to evaporate SiO₂, which otherwise could be worth testing as an alternative for SiN.

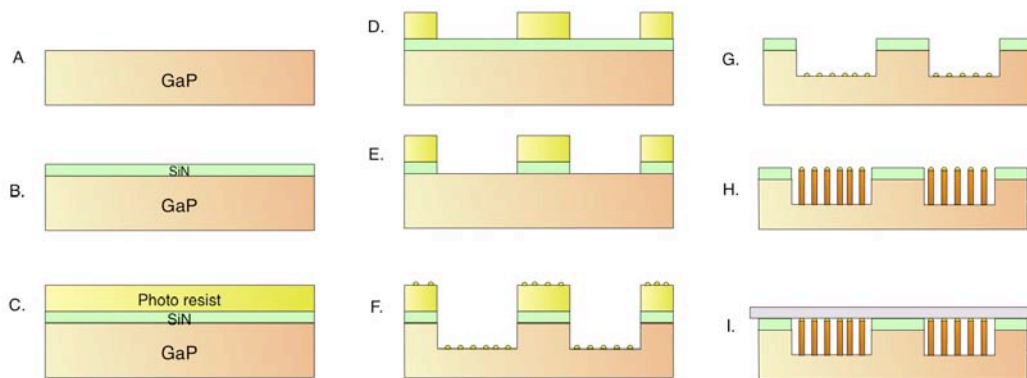


Figure 4.11: Scheme for producing etched channels with nanowires. (A) A GaP wafer. (B) SiN deposition. (C-D) Channels are fabricated in a photo resist (Shipleys S1813). (E) The pattern is transferred to the GaP substrate using RIE. (F) Wet etching and deposition of gold particles. (G) Photo resist is removed and so are all gold particles on top of the channels. (H) Nanowire growth. (I) Sealing with plain PDMS sheet.

Results and discussions of wet etching

We managed to etch trenches in GaP with a standard recipe for etching GaInAs and InP (described in appendix A). The depth of the trenches was ~200nm, which after subtraction of the ~80nm SiN layer gives an etching rate of ~6nm/min for our 20min of etching (see figure 4.12). The parabolic etching profile is typical to wet etching and due to non-depletion of etchant molecules over the etching mask, where there is a higher concentration of etchant molecules that easily diffuse and etch close to the edges.

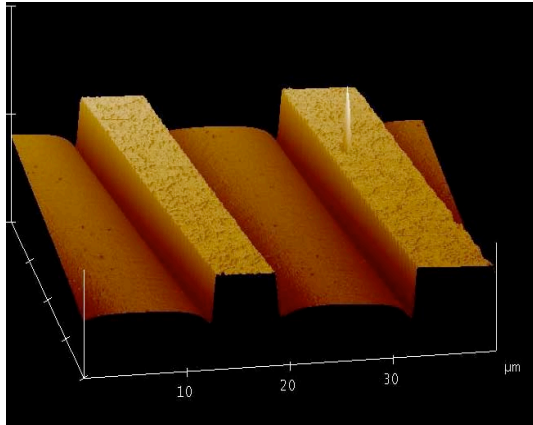


Figure 4.12: AFM image showing GaP channels etched in bromine water. The depth is around 200nm and the channels are 10 μ m wide.

To get higher etch rates, we used an etchant consisting of bromine and methanol for 6min (see appendix A for details). Several μ m were etched and the etching mask worked fine, but the surface was very rough. Figure 4.13 shows that the etching takes place in all 111 directions ((111), (11 $\bar{1}$), (1 $\bar{1}$ $\bar{1}$) and so on) and pits are formed. A subsequent wet etch with the bromine water recipe did not smoothen the surface. Note that the SiN layer was not etched at all and seems to hang out over the undercut (figure 4.13). This phenomenon could be used to fabricate SiN cantilevers.

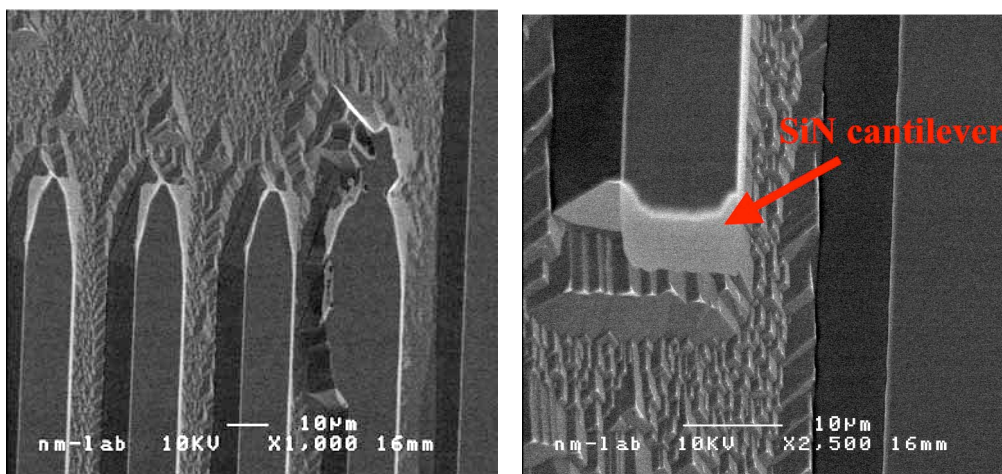


Figure 4.13: 30° tilted SEM images after 6 min etching with Br:MetOH solution. The etched surface is very rough with small pits. The right image clearly shows SiN hanging out over the undercut.

Results and discussion of nanowire growth in etched GaP channels

Straight GaP nanowires were successfully grown in etched GaP channels. The photo resist was removed before deposition of gold particles to investigate the etching profile. Therefore there is also growth outside the channels on the SiN and we could not use these devices for bonding to PDMS and flowing DNA. The nanowires are \approx 400nm long, about half the size from nanowires grown simultaneously on wafers

without channels. A plain wafer etched with the same bromine water recipe had twice as long nanowires, which indicates that it is the geometry of the channels that gives a slower growing rate. Probably, a large amount of growth material gets into the edges in the hyperbolic channels. More tests with growth in deeper channels are needed before making conclusions about how nanowire growth depends of the geometry of channels.

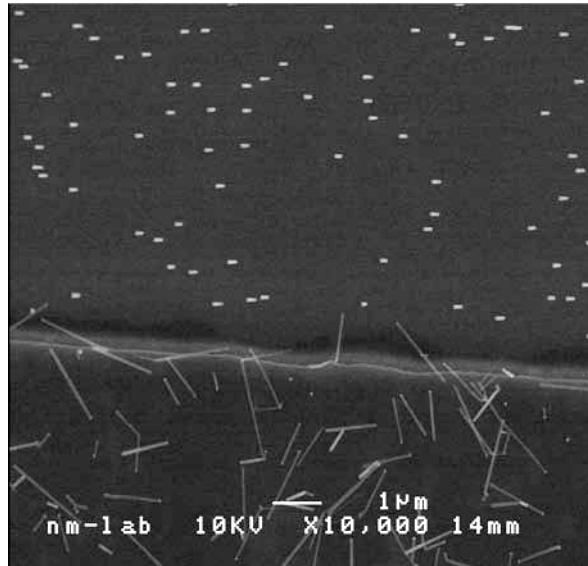


Figure 4.14: 30° tilted SEM image of nanowires grown in etched GaP channels. This is the same device as in figure 4.12.

A somewhat unsuccessful sample with etched channels got the peculiar etching profile shown in figure 4.15 (note that the undercut is not shown in an AFM image). The deepest parts of the channels are about 170nm and the width is $\approx 10\mu\text{m}$. Nanowire growth on this sample was successful with long straight nanowires (figure 4.16) and this shows that macroscopic notching effects are not always critical for nanowire growth. Observe the different scales in figure 4.15:right; the inclination in the channel between the green arrows is less than 1%. Still, it is important knowledge that straight wires can be grown on non-flat surfaces.

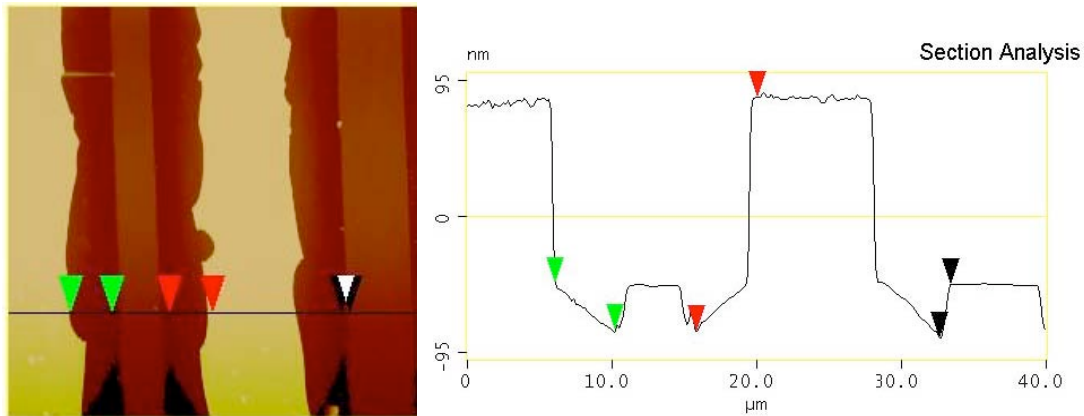


Figure 4.15: AFM image of peculiar, etched channels in GaP. (left) Topview. (right) Cross section showing the etching profile. Observe the difference in scale.

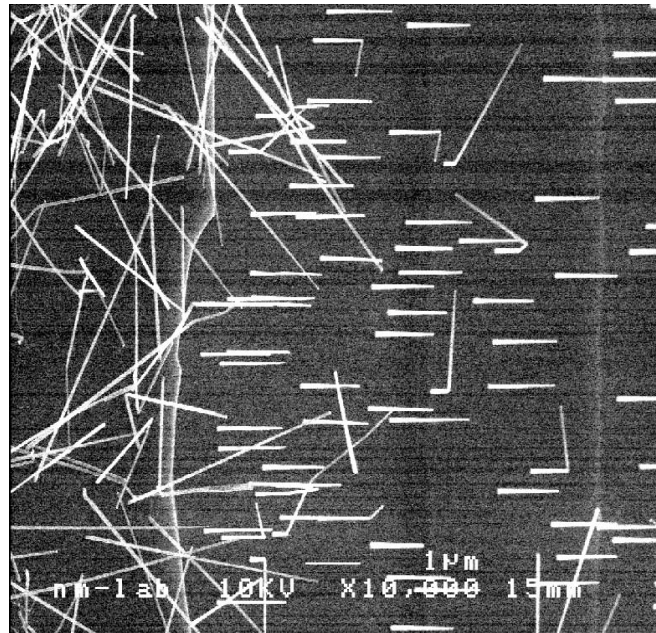


Figure 4.16: 30° tilted SEM image of nanowires grown on the same device as in figure 4.15. The nanowires are $\approx 2\mu\text{m}$ long.

The procedure of growing nanowires in etched GaP channels described in this chapter gives no growth outside the channels. However, if we want to grow nanotrees instead of nanowires, this method is not suitable. The photo resist must be removed before the first growth process and there will therefore get gold particles outside the channels in the second deposition. RIE could be used to remove the silicon nitride layer and could also have removed the lying nanowires outside the channels. However, tests show that the nanowires instead acted as an etch mask and stayed on the surface (figure 4.17). It is not bumps in the SiN, but nanowires, we see in figure 4.17, because we have etched down all the way to the GaP layer. This means that we can etch SiN selectively over GaP, which can be useful for other purposes. However with an etching method with larger undercut, one should be able to remove

lying nanowires on the surface. One could also fill the channels with a resist and etch away GaP outside channels before removing the resist again. This method and alternative methods of growing nanotrees in channels are discussed in Ch6.

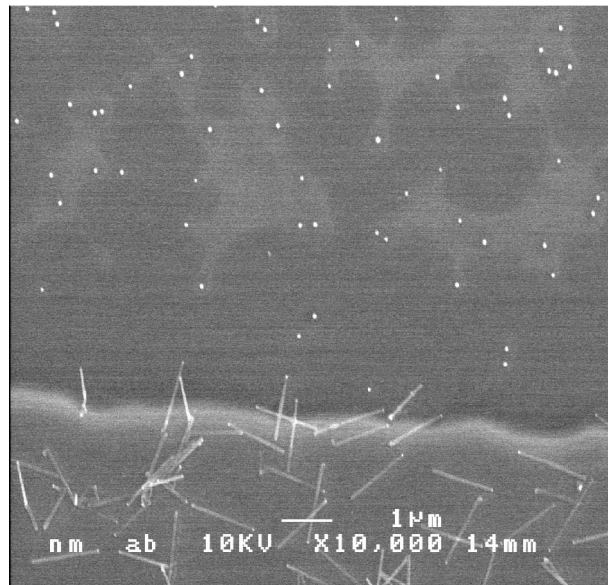


Figure 4.17: SEM image of the sample in figure 4.12 after RIE. Growth outside channels was not removed.

Conclusion

The successful growth in etched GaP channels is very promising for future applications and when we have devices without growth outside the channels, bonding to PDMS will be possible and a flow around the nanowires can be investigated.

4.4.2 Growing GaP nanowires in etched silicon channels

Method

We do not need a layer of SiN, because natural silicon bonds to PDMS after oxygen ashing. This was shown and explained in section 3.1.

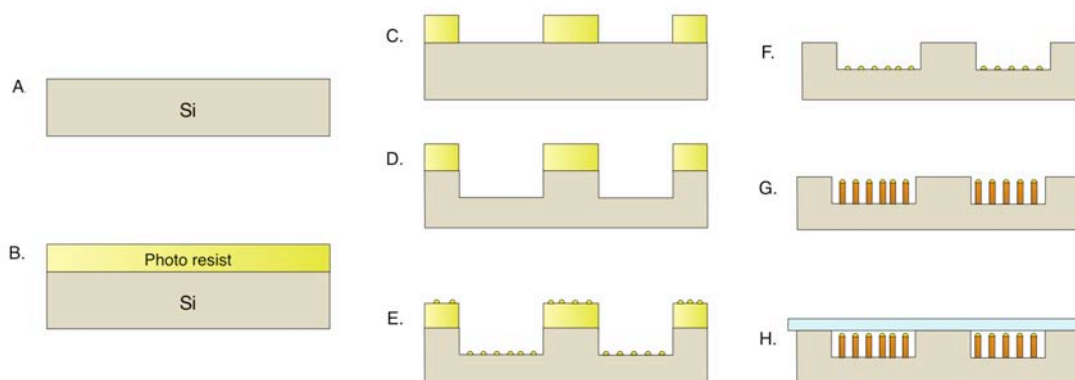


Figure 4.18: Method of growing GaP nanowires in etched silicon channels that provide bonding. (A) A plain Si wafer. (B-C) Channels are fabricated in a photo resist (Shipley's S1813). (D) RIE in silicon. (E) Deposition of gold particles. (G) Photo resist is removed and so are all gold particles on top of the channels. (H) Nanowire growth. (I) Bonding to a plain PDMS sheet.

Nanowire growth on silicon is not yet fully understood and optimized even on non-etched surfaces. Therefore, five different procedures were tested to investigate how different processing steps affect the growth on silicon. Hydrofluoric acid (HF) etch is sometimes used to remove oxidized layers on the devices between alternating steps. Photo resist could influence gold particle deposition and removal of photo resist could affect the particles and the surfaces before nanowire growth. Therefore, we tested to both keep the photo resist during gold particle deposition and to remove it before. These methods were investigated:

1. Photo resist kept during gold deposition; 10s wet HF etch before deposition
2. Photo resist kept during gold deposition; HF etch before nanowire growth
3. Photo resist kept during gold deposition; no HF etch
4. Photo resist removed before gold deposition; HF etch before deposition
5. Photo resist removed before gold deposition; no HF etch

After growth, the device is bonded to PDMS after 60s oxygen plasma treatment and DNA is flown through the channels as described in section 4.0.

Results and discussion of etching and growth in etched channels in Si

Nanowires were grown in all five methods. Since we grew on (110) oriented substrates, we did not expect nanowires to be vertical to the substrate. However, the nanowires did not only grow in the $\langle 111 \rangle$ directions, but in all kinds of directions and some areas did not get any growth at all. There were no significant differences

between the methods except from growth outside the channels whenever the photo resist was removed before gold deposition and also that some areas with gold particles seemed to have been removed during HF etch in method 2.

The nanowires grew in all directions probably because the surface was not smooth enough and perfectly clean. The crystal orientation of the substrate is therefore not well defined and it is no longer energetically favourable to grow only in the $\langle 111 \rangle$ directions. The etched surface was actually rather rough after RIE and our processing steps before nanowire growth probably make the surface somewhat dirty.

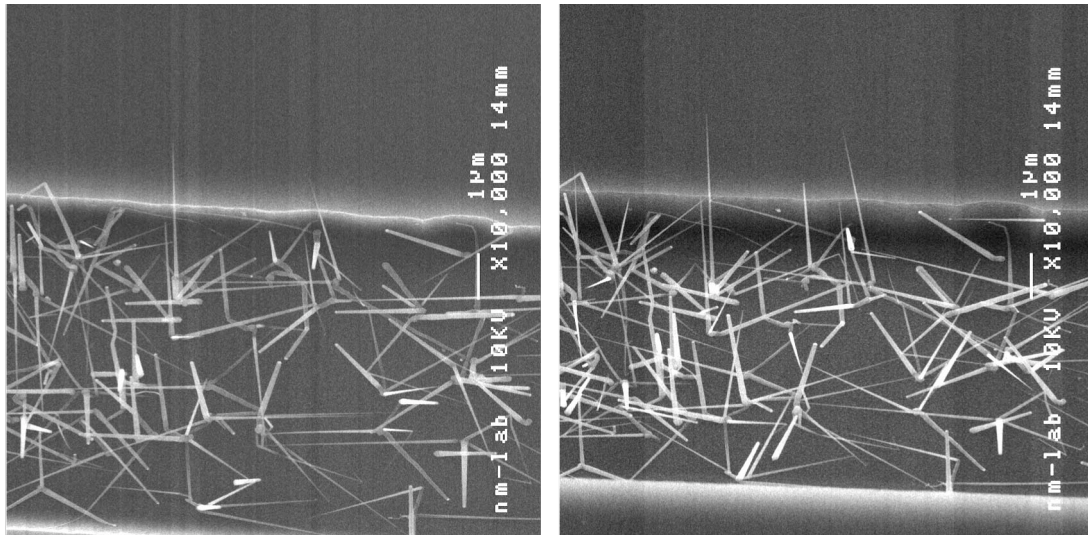


Figure 4.19: SEM image of nanowires grown in Si channels. (left) Topview. (right) 30° tilted view of the same area. We did a 10s HF etch before Au deposition. The photo resist was removed after the deposition.

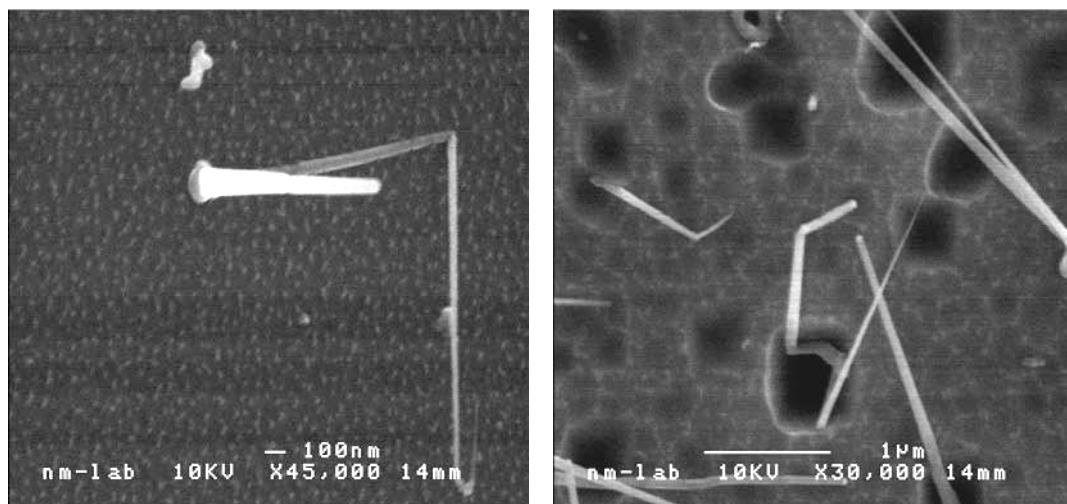


Figure 4.20: SEM images tilted 30° showing the rough surface after RIE. Still, a nanowire has managed to grow seemingly straight up (left image).

Both figure 4.19 and figure 4.20 show several nanowires growing from the same spot and in figure 4.21 there are more examples, marked with red circles. There seems like

only one of all nanowires from a single spot has a gold particle on its top. The growth is thus initiated under the seed particle, but proceeds without particles on top of all nanowires. This does not agree with either of the models for nanowire growth described in the theory section and shows that this field of research still has many fundamental questions to investigate. The nanowires without particles on top also are much longer than usual and become thinner at the ends.

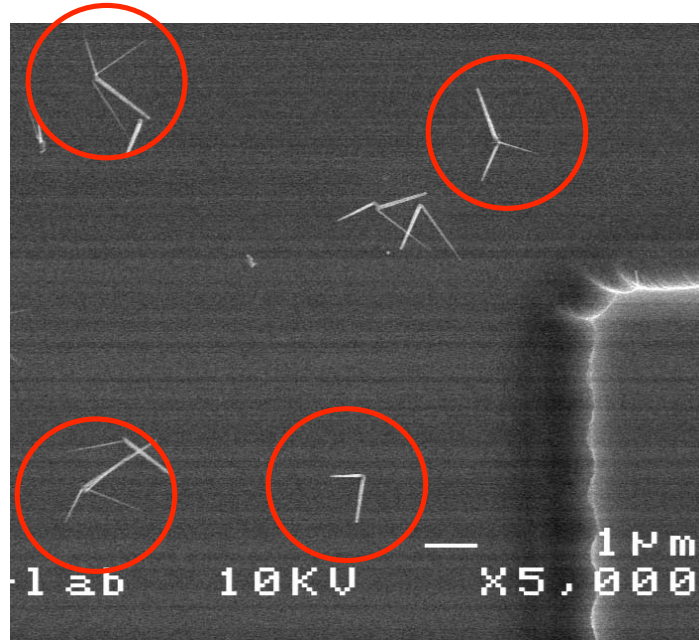


Figure 4.21: SEM images of several nanowires grown from the same spots. This device was made from method no2.

Results and discussion of DNA flowing in Si channels containing nanowires

The device from method three (figure 4.22) was used for flowing DNA in the channels with nanowires and it worked very well. The bonding succeeded and we could not detect any leakages. Further, we could see DNA stretching out around the nanowires when flowing in the channels. Much DNA only stretches a few micrometer before loosing the grip of the nanowire and continuing with the flow. Other DNA strands get stuck on nanowires and stretch out 9-19 μm . Fully stained λ -DNA is 21 μm long, so the DNA stretches out a considerable amount of its own length. There were also multimers of DNA stretching out up to 48 μm , still without damaging the nanowires. We also noted that DNA stretched more when they had one end on each side of a nanowire than when stretched only from one end.

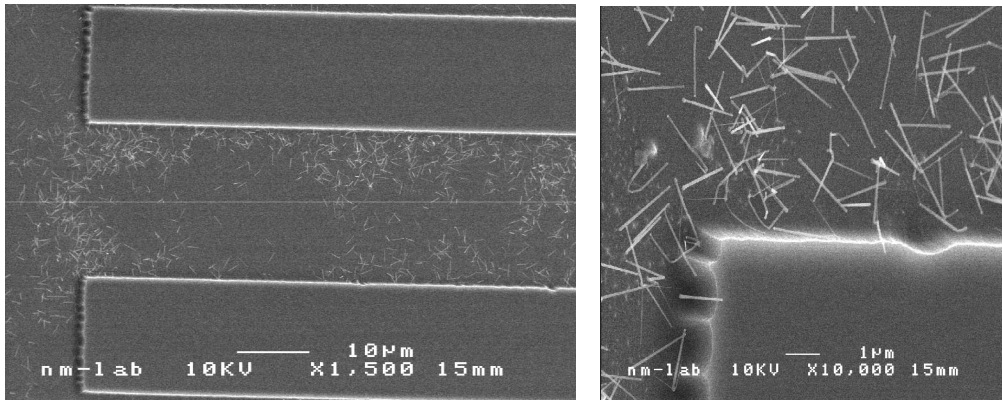


Figure 4.22: SEM images of device used in this experiment. (left) Topview at 1.5kX. (right) 30° tilted image at 10kX.

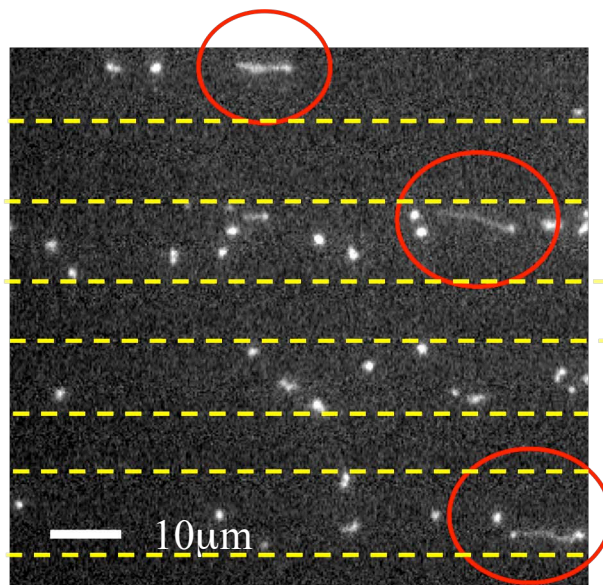


Figure 4.23: DNA stretched out while flowing in the channels. Yellow dashed lines show the boundaries of the channels, which are difficult to detect, because Si does not fluoresce.

Conclusion

We knew already that it is not trivial to grow perfect nanowires on silicon. The fact that all five different procedures in this first attempt led to nanowires in channels is very promising. The etched surface can be improved by changing RIE recipe or using wet etching or other etching methods and this would probably improve the result of nanowire growth significantly. However, in Ch 6 we will discuss advantages of tilted nanowires (and nanotrees) in channels and how this can be used in a novel separation device. Further, we saw growth of several nanowires from single gold particles, which cannot be explained with current growth models.

We were delighted to see DNA stretching out around the tilted nanowires in a device without leakages. It is promising that the silicon method was successful, both because silicon devices are preferred in future applications and also because the method includes less steps than the GaP method.

5. Conclusion

In conclusion, we have integrated nanowires and microfluidics using three different methods:

- **GaP nanowires in etched silicon channels and oxygen bonding**
 - + The device worked fine and DNA stretched out around the nanowires
 - + There were more than 90% bonding
 - +/- The nanowires were not straight, however this could be an advantage
 - The nanowire growth needs improvement
- **SU8 channels around GaP nanowires grown on GaP and bonding to PMMA in a nano imprint machine**
 - + Nice flow with DNA stretching out around the nanowires
 - There were approximately 10% bonding
 - The bonding needs to be improved
- **SU8 channels around GaP nanowires grown on GaP with subsequent SiN deposition and bonding to PDMS after oxygen ashing**
 - + The device worked for a long time and the bonding did not deteriorate
 - DNA did not seem to stretch out
 - There were approximately 30% bonding
 - The bonding needs to be improved

Further, straight nanowires were grown in etched GaP channels with great yield. With improved etching methods, dense arrays of GaP nanowires can be grown and integrated with micro flows after bonding to PDMS.

Tilted nanowires were grown in etched silicon channels and we saw several nanowires grown from single seed particles. We believe there were nanowires without gold particles on top, showing that present models for nanowire growth are yet to be improved.

Bonding is still an issue and needs to be improved. Generic bonding methods would enable development of new methods where materials can be chosen with consideration of other issues such as conductivity, growth ability or transparency.

For future applications a more controlled flow system is desired. Electrophoresis would be preferred over pressure driven flows, because higher flow rates can be obtained when downscaling. The GaP method used in this project uses materials that should be sufficiently non-conducting to provide electrophoresis. In the other method, the silicon must be oxidized or modified in some way to become isolating before using electrophoresis.

6. Outlook

6.1 Growth of branched nanostructures in etched silicon channels

6.1.1 Method no.1

The natural continuing step is to integrate branched nanostructures with microfluidic systems. Figure 6.1 shows a method similar to the ones used in this project with the difference that a protecting layer of material x prevents growth on the surface needed for bonding. After all growth steps, material x is etched away. Material x therefore needs to be chosen such that it can be etched selectively over GaP and gold and preferably with large undercut so that all growth on the surface is removed.

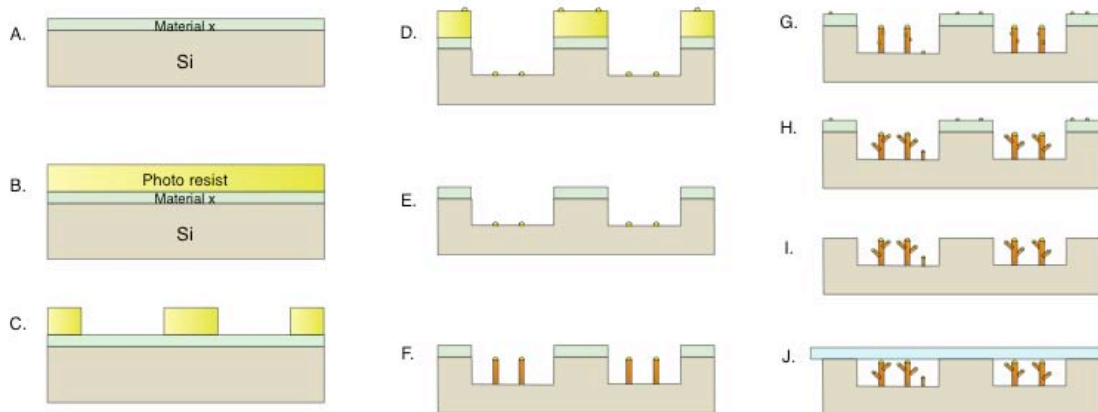


Figure 6.1: Scheme for growing nanotrees in etched silicon channels with removal of nanowire growth outside channels after the growth.

6.1.2 Method no.2

Another method to remove growth outside the channels is to fill the channels with a resist and then etch GaP to remove growth outside the channels. A subsequent HF etch would remove gold particles on the surfaces. Finally the resist is removed. (figure 6.2)

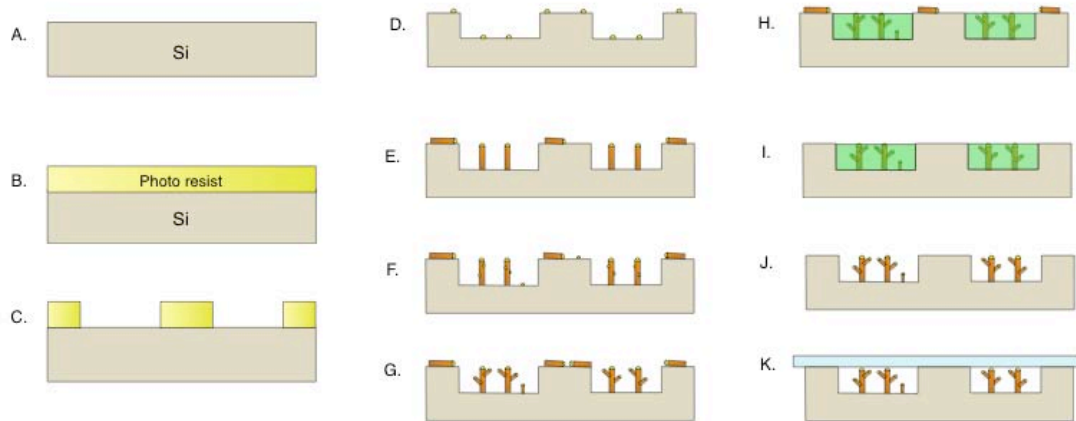


Figure 6.2: Scheme for growing nanotrees in etched silicon channels. Material x must withstand the harsh environment in MOVPE and be able to etch selectively over GaP and gold.

6.2 Future Applications

6.2.1 Novel topological separator for DNA

In this project, we saw DNA stretching out around tilted nanowires. This can be used for separation of circular from non-circular DNA. Circular DNA, or plasmids, are widely used in gene therapy, where desired genes are incorporated into plasmids, which then are used to fight diseases. The plasmids should be supercoiled and this method would quickly both give a number of and increase the concentration of supercoiled DNA in a sample containing plasmids. Both the circular DNA and non-circular or supercoiled DNA are collected via separate outlets. The device can also be used for studying amounts of supercoiled DNA in different buffers etc. [28]

Circular DNA would get stuck around the nanowires, whereas the non-circular DNA stretches out and continues as we have shown here. Instead of tilted nanowires, we can also use nanotrees grown in channels according to the method described above.

With asymmetric nanotrees or nanowires all tilted in the same direction, the circular DNA can be collected by reversing the flow direction as shown in figure 6.3. It should be possible to grow tilted nanowires on (110) surfaces to realize this device. Fabrication of asymmetric nanotrees has been should also be possible in the future.

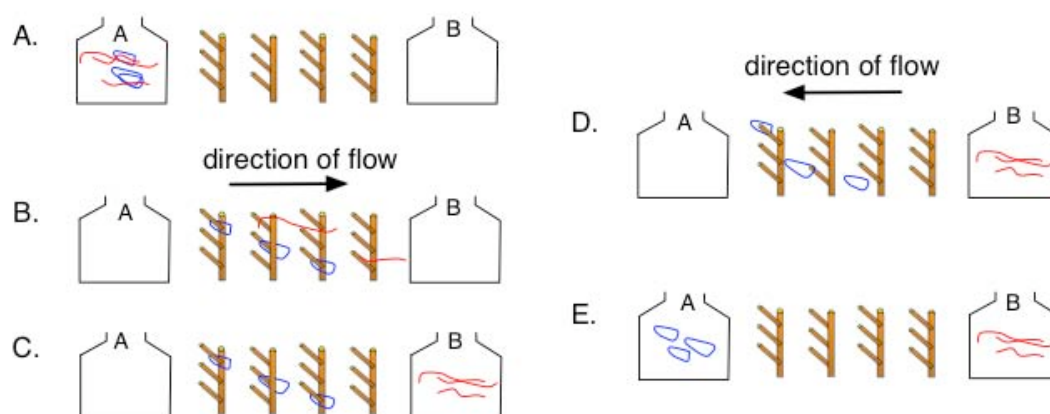


Figure 6.3: A novel method of separating circular DNA from non-circular DNA in an array of asymmetric nanotrees (or tilted nanowires). (A) All DNA in beaker A. (B) circular DNA get stuck around the nanotrees. (C) Non-circular DNA is collected in beaker B. (D) Circular DNA is removed from the nanotrees by reversing the flow direction. (E) The circular DNA is collected in beaker A and the separation is finished.

6.2.2 Protein separator - Bumper array

Another step forward would be to integrate nanowires in specific patterns with microfluidics. In 2004, Huang et al. presented a novel method of separating particles with respect to size. This method is fast compared to other separation techniques and you actually get less spread for higher speeds because you decrease diffusion. The separation uses lateral displacement, i.e. one can run the device continuously and collect different sized particles with different outlets. [29]

Figure 6.4 shows how the method works; an array of obstacles forces large particle to follow the inclination of that array, whereas small particles follow the laminar flow. The separation between posts, size of the posts and period of the array determine the cut of size (R_c) above which particles start to bump.

$$R_c = \alpha \frac{d}{N}, \text{ where } d \text{ is distance between posts,}$$

N is the period and α is a correction factor

With an array of nanowires with $d=40$, $N=10$ and $\alpha=2.5$, the cut off size is 10nm and proteins can be separated with respect to size.

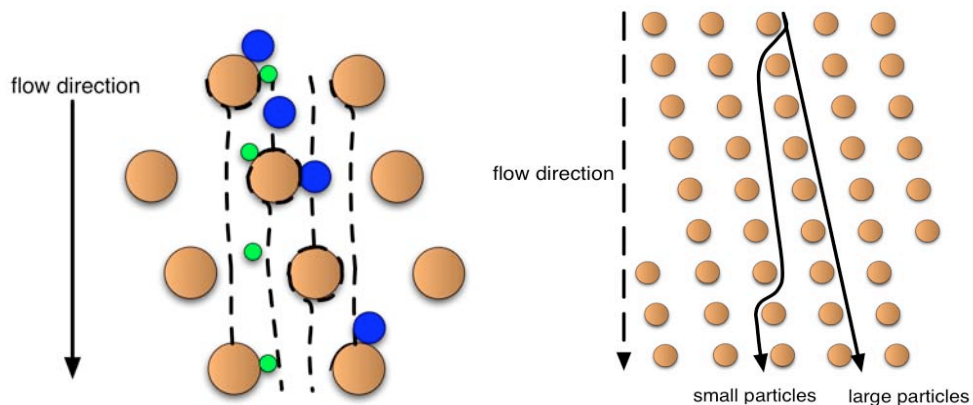


Figure 6.4: The method of the bumper array. Small particles follow the laminar flow and large particles are forced to follow the inclination of the array.

6.2.3 Biosensor using oscillating nanowires

Nanowires has shown to be strong and can be bended and oscillated as springs without breaking, recently shown by M. Lexholm in her Master thesis [30]. If the mass of the nanowire changes, there will be a shift in their resonance frequency very much like for cantilevers [31]. By detecting frequency shift, one can thus measure adsorption of biomolecules to the nanowire. To be able to provide a natural environment for the biomolecules, integration with microfluidics is necessary and that gives a strong connection to this project. By investigating the decay curve of the oscillation, we can get information of the dissipation of the attached molecules. The measured adsorbed mass includes water content, simultaneous SPR measurements (Surface Plasmon Resonance), which do not include that water, would therefore provide important additional information. This should be possible with our normal seed particles made of noble materials. [32]

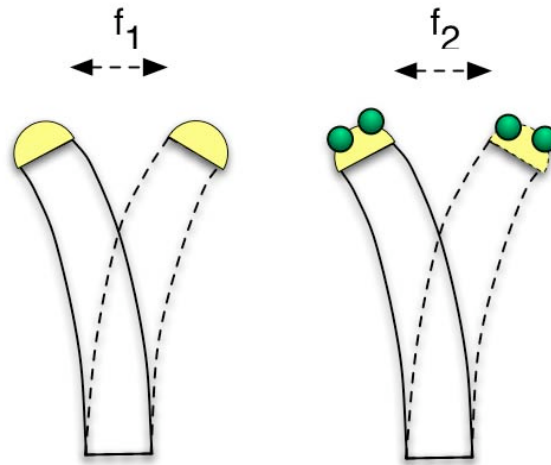


Figure 6.5: (left) a nanowire oscillating at its resonance frequency f_1 . (right) Adsorbed molecules give a frequency shift to f_2 and the adsorbed mass can be determined. Simultaneous SPR measurements will give additional important information.

6.2.4 Surface area enhancer

A dense forest of nanowires or nanotrees has a very large surface/volume ratio and this can be used as a surface area enhancer. When the molecules flow past an adsorption area, in for example a sensor with fluorescent detection, they need to get close to the surface to bind. By increasing the surface area without increasing the volume that area enclose, the probability of adsorption increases. We have thus increased the sensitivity and are able to measure lower concentrations.

7. References

1. Jonas O. Tegenfeldt, Christelle Prinz, Han Cao, Richard L. Huang, Robert H. Austin, Stephen Y. Chou, Edward C. Cox, James C. Sturm, *Micro- and nanofluidics for DNA analysis*. Anal Bioanal Chem, (378): p. 1678-1692 (2004)
2. Allon I. Hochbaum, Rong Fan, Rongrui He and Peidong Yang, *Controlled Growth of Si Nanowire Arrays for Device Integration*. Nanoletters, (2004)
3. T. Mårtensson, P. Carlberg, M Borgström, L Montelius, W. Seifert, L. Samuelsson, *Nanowire Arrays Defined by Nanoimprint Lithography*. Nanoletters, 4(4): p. 669-702 (2004)
4. C. Thelander, H. A. Nilsson, L. E. Jensen and L. Samuelsson, *Nanowire Single-Electron Memory*. Nanoletters, 5(4): p. 635-638 (2005)
5. Hernán, Tania, *Growth and characterization of GaAs/(AlIn)P core/shell nanowires with subsequent conversion into hollow tube structures*, Master of Science thesis, Solid State Physics at Lund University, Lund (2005)
6. Guowen Meng, Yuond Joon Jung, Anyuan Cao, Robert Vajtai and Pulickel M. Ajayan, *Controlled fabrication of hierarchically branched nanopores, nanotubes and nanowires*. PNAS, 102(20): p. 7074-7078 (2005)
7. Kimberley Dick, Knut Deppert, Magnus W. Larsson, Thomas Mårtensson, Werner Seifert, L. Reine Wallenberg and Lars Samuelsson, *Synthesis of branched 'nanotrees' by controlled seeding of multiple branching events*. Nature materials, (3): p. 380-384 (2004)
8. Giddings, J. C., *Unified Separation Science*. 1991.
9. J. R. Welty, R. E. Wilson, C. E. Wicks, *Fundamentals of Momentum Heat and Mass Transfer*. 2 ed. 1976.
10. David J. Beebe, Glennys A. Mensing, and Glenn M. Walker, *Physics and Applications of Microfluidics in Biology*. Annu. Rev. Biomed. Eng., (2002)
11. A. Kolmakov, D. I. Klenov, Y. Lilach, S. Stemmer and M. Moskovits, *Enhanced Gas Sensing by Individual SnO₂ Nanowires and Nanobelts Functionalized with Pd Catalyst Particles*. Nanoletters, 5(4): p. 667-673 (2005)
12. Borgström, Magnus, *Epitaxial Growth, Processing and Characterization of Semiconductor Nanostructures*, Doctoral thesis, Solid State Physics at Lund Institute of Technology, Lund University, Lund (2003)
13. Björk, Mikael, *Electron Transport in Semiconductor Nanowires*, Doctoral thesis, Solid State Physics at Lund Institute of Technology, Lund University, Lund (2004)
14. <http://www.warwick.ac.uk/~phsbm/mbe.htm>, *Layered Growth of Semiconducting Materials*.

15. Kimberly A. Dick, Knut Deppert, Thomas Mårtensson, Bernhard Mandl, Lars Samuelson, and Werner Seifert, *Failure of the Vapor-Liquid-Solid Mechanism in Au-Assisted MOVPE Growth of InAs Nanowires*. Nanoletters, 5(4): p. 761-764 (2005)
16. Ann I. Persson, M. W. Larsson, S. Stenström, B. J. Ohlsson, L. Samuelsson and L. R. Wallenberg, *Solid-phase diffusion mechanism for GaAs nanowire growth*. Nature materials, 3: p. 667-681 (2004)
17. Madou, Marc J., *Fundamentals of Microfabrication- The Science of Miniaturization*. 2 ed. 2002, London, New York, Washington D.C.: CRC Press.
18. <http://www.iljinnanotech.co.kr/en/material/r-4-3.htm>, Synthesis methods, Nanotech, Iljin, 2005-07-14
19. John L.Vossen, Werner Kern, *Thin Film Processes*. 1978, New York, San Francisco, London: Academic Press.
20. Samuel K. Sia, George M. Whitesides, *Microfluidic devices fabricated in poly(dimethylsiloxane) for biological studies*. Electrophoresis, (24): p. 3563-3576 (2003)
21. Round, Andy, *Scanning Probe Microscopy at Bristol*, University of Bristol.
22. Center for Materials Research and Analysis University of Nebraska-Lincoln[Nebraska-Lincoln, #24], <http://www.unl.edu/CMRAcfem/semoptic.htm>.
23. Mårtensson, Thomas, *EBL Defined Whisker Arrays*, Master thesis, Solid State Physics at Lund University, Lund (2003)
24. <http://micro.magnet.fsu.edu/primer/techniques/fluorescence/fluorhome.html>, the Optical Microscopy Division of the National High Magnetic Field Laboratory, The Florida State University, the University of Florida, and the Los Alamos National Laboratory, 2005-08-28
25. B Bilenberg, T Nielsen, B Clausen and A Kristensen, *PMMA to SU-8 bonding for polymer based lab-on-a-chip systems with integrated optics*. Journal of Micromechanics and Microengineering, (14): p. 814-818 (2004)
26. S Liu, JB Tok, and Z Bao, *Nanowire lithography: fabricating controllable electrode gaps using Au-Ag-Au nanowires*. Nanoletters, 5(6): p. 1071-1076 (2005)
27. BK Agrawal, S Agrawal, and S Singh, *Ab-initio study of the structural and electronic properties of very thin silver nanowires*. J Nanosci Nanotechnol, 5(4): p. 635-640 (2005)
28. G. N. M. Ferreira, G. A. Monteiro, D. M. F. Prazeres and J. M. S. Cabral, *Downstream processing of plasmid DNA for gene therapy and DNA vaccine applications*. Trends in Biotechnology, 18(September): p. 380-388 (2000)
29. L. R. Huang, E. C. Cox, R. Austin and J. C. Sturm, *Continuous Particle Separation Through Deterministic Lateral Displacement*. Science, 304: p. 987-990 (2004)
30. Lexholm, Monica, *Interference in the nanoworld*, Master thesis, Solid State Physics at Lund University, Lund (2005)
31. Ghatnekar-Nilsson, Sara, *Nanomechanical Studies and Applications of Cantilever Sensors*, Doctoral thesis, Solid State Physics at Lund University, Lund (2005)
32. Charlotte Larsson, Michael Rodahl and Fredrik Höök, *Characterization of DNA Immobilization and Subsequent Hybridization on a 2D Arrangement of Streptavidin on a Biotin-Modified Lipid Bilayer Supported on SiO₂*. Anal. Chem, 75(19): p. 5080-5087 (2003)

Appendix A-Processing parameters and recipes

Recipe for Photolithography with Shipley S1813

1. Cleaning	Acetone and Isopropanole on the spinner
2. Spinning	5600rpm for 45s (high acceleration)
4. Soft bake	115°C in 90s on hotplate
5. Exposure	8s at 12.5mW/cm ² \Leftrightarrow \approx 100mJ/cm ² (λ =365nm and 405 nm)
6. Development	1min in MF319
7. Rinsing	DI water

Recipe for Photolithography with SU8

Processing of SU8-2005 from Microchem for a thickness of 2 μ m.

1. Cleaning	Acetone and Isopropanol on the spinner
2. Prebake	200°C in an oven for at least a few hours
3. Spinning	5750rpm for 45s (high acceleration)
4. Soft bake	1min on 65°C hotplate 2min on 95°C hotplate
5. Edge bead scraping	Scrape of edge bead with scalpel (cooling of sample at the same time)
6. Exposure	7s at 12.5mW/cm ² \Leftrightarrow \approx 90mJ/cm ² (λ =365nm and 405 nm)
7. Post Exposure Bake	30min on 65°C hotplate
8. Development	1min in SU8 Developer
9. Rinsing	Rinse in Isopropanol and dry with N ₂
10. Hard bake	Bake for two hours in 200°C oven

Recipe for wet etching with Bromine water

A standard recipe for etching in GaInAs and InP was used. Etching rate is appr. 1-2nm/s for these materials.

1. Cleaning
 2. Etchant solution
 3. Etching
 4. Rinsing
 5. Cleaning
- Clean plastic beakers in MilliQ-water
pour 40 ml of DI water into a plastic bottle
add 0.3ml SBW (saturated bromine water, shake bottle first)
add 5ml HBr (47%)
add 5ml HNO₃ (nitric acid) (65%)
Put your sample into the etchant solution with a teflon pipette and stir gently.
Rinse in plastic beaker with MilliQ water and then under floating MilliQ water.
Sample in small beaker with Acetone on 50°C hotplate for a couple of minutes. (be aware of the risk of fire)
Do the same with Isopropanole.
Dry immediately with N₂.

Recipe for wet etching with Br:MetOH

Etching rate for GaP was appr. 1µm min.

1. Cleaning
 2. Etchant solution
 3. Etching
 4. Rinsing
 5. Cleaning
- Clean plastic beakers in MilliQ-water
pour 200 µl of bromine into a plastic beaker
add metanol to a total volume of 20ml
Put your sample into the etchant solution with a teflon pipette and stir gently.
Rinse in pure metanol for 60s
then with MilliQ water for 60s and then under floating MilliQ water for 10s
Sample in beaker with Acetone on 50°C hotplate for a couple of minutes. (be aware of the risk of fire)
Do the same with Isopropanole.
Dry immediately with N₂.

Parameters for PECVD of Silicon Nitride

Deposition of $\text{Si}_x\text{N}_y\text{H}$ for an isolating layer with thickness of about 84nm and index of reflection of about 2. Deposition rate is about 28nm/min.

Temperature	$T=350^\circ\text{C}$
Flows	300ml/min of 5% SiH_4 + 15 ml/min of 95% N_2
Time	$t=36$
Power	$P=60\text{W}$
Pressure	$p=80\text{Pa}$ (600mTorr)
Frequency	$f=13.56\text{Hz}$
Current	$I=5.3\text{A}$

Parameters for RIE in Silicon Nitride

These parameters were used for an etch rate $> 1.17\text{nm/s}$ in SiN.

Flow	CF_4 100 ml/min
	O_2 10ml/min
Pressure	$p=8.7\text{Pa}$ (65mTorr)
Power	$P=25\text{W}$
Current	$I=2.6\text{A}$
Voltage	$U=230\text{V}$

Parameters for RIE in silicon

These parameters were used for etching appr. $1.1\mu\text{m}$ in Si.

Flow	SF_6 25 ml/min
	O_2 20ml/min
Time	100s
Pressure	$p=6.7\text{Pa}$ (50mTorr)
Power	$P=100\text{W}$
Current	$I\approx 5\text{A}$
Voltage	$U\approx 400\text{V}$

Recipe for bonding with Nanoimprint machine

- | | |
|-----------------------|--|
| 1. Prebake glass | Bake your glass on a 160°C hotplate for at least 10min |
| 2. Adhesion promoting | Spin on an adhesion promotor (AP300) and bake for 90s on a 115°C hotplate |
| 3. Spinning | Spin on PMMA 950k a5 at 2000rpm for 45s |
| 4. Soft bake | Bake on 150°C hotplate for 10min |
| 5. Bonding | Place your sample on the PMMA with the SU8 facing down
Heat the sample and then add pressure for 10min. Keep the pressure until cooling to 80°C |

Bonding parameters

Temperature	110°C
Pressure	1MPa (10bar)
Time	10min
Cooling temperature	80°C

Recipe for DNA buffer

This is a recipe for making buffer for DNA and dilution of DNA.

54 g Tris base → 450mM

27.5 g Boric acid → 440 mM

add distilled water to 0.8L

titrate with sodium hydroxide (NaOH) to pH8.5

Appendix B

Differential representation of fluid flow

A set of differential equations representing a general flow system is a convenient starting point for more specific cases, where boundary conditions and such can be used to derive more hands-on equations. Reference for this whole appendix is “Fundamentals of Momentum Heat and Mass Transfer” by Welty, Wilson and Wicks [9] and “Unified separation science” by Giddings [8].

The Continuity equation

Due to conservation of mass, the rate of mass flux in to a small control volume ($\Delta V = \Delta x \Delta y \Delta z$) must equal the rate of accumulated mass within the same volume, which gives:

$$\iint_{\text{control surface}} \rho \mathbf{v} \cdot \mathbf{n} dA + \frac{\partial}{\partial t} \iiint_{\text{control volume}} \rho dV = 0, \quad \text{B-1}$$

where ρ is the density, \mathbf{v} velocity and \mathbf{n} direction

The mass flux in x -direction over cross section $\Delta y \Delta z$ is $\rho(v_x|_{x+\Delta x} - v_x|_x) \Delta y \Delta z$. Divide by ΔV and let $\Delta x, \Delta y, \Delta z \rightarrow 0$ and we get:

$$\sum_{i=x,y,z} \left(\frac{\partial}{\partial i} (\rho v_i) \right) + \frac{\partial \rho}{\partial t} = 0 \quad \text{B-2}$$

The sum is the divergence of $\rho \mathbf{v}$ and the relation $\text{div} \mathbf{a} = \nabla \cdot \mathbf{a}$ gives the continuity equation:

$$\nabla \cdot (\rho \mathbf{v}) + \frac{\partial \rho}{\partial t} = 0 \quad \text{B-3}$$

For an incompressible fluid the density ρ does neither change with time nor in space and the continuity equation is reduced to:

$$\nabla \cdot \mathbf{v} = 0 \quad \text{B-4}$$

The Navier-Stokes equations

Newton's second law of motion ($F=ma$) applied to fluids is called the Navier-Stokes equations. Consider a small control volume ($\Delta V=\Delta x\Delta y\Delta z$) and make a similar discussion to the one above about conservation of mass.

All external forces must equal the net rate of linear momentum efflux + the time rate of change of linear momentum within the control volume. This can be described as:

$$\sum_{\text{external forces}} F = \iint_{\text{control surface}} \rho \mathbf{v}(\mathbf{v}\mathbf{n})dA + \frac{\partial}{\partial t} \iiint_{\text{control volume}} \rho \mathbf{v}dV \quad \text{B-5}$$

External forces

Let us first look at the left side of the equation above. The force component in x-direction is:

$$\begin{aligned} \sum F_x = & \left(\sigma_{xx}|_{x+\Delta x} - \sigma_{xx}|_x \right) \Delta y \Delta z + \left(\tau_{yx}|_{y+\Delta y} - \tau_{yx}|_y \right) \Delta x \Delta z + \\ & \left(\tau_{zx}|_{z+\Delta z} - \tau_{zx}|_z \right) \Delta x \Delta y + g_x \rho \Delta V \end{aligned} \quad \text{B-6}$$

normal stress shear stress in y-direction
shear stress in y-direction gravitational component

We can divide by ΔV , which is constant and let $\Delta x, \Delta y, \Delta z \rightarrow 0$:

$$\frac{\sum F_x}{\Delta V} = \frac{\partial \sigma_{xx}}{\partial x} + \frac{\partial \tau_{yx}}{\partial y} + \frac{\partial \tau_{zx}}{\partial z} + g_x \rho \quad \text{B-7}$$

Let us now look at first term on the right hand side of equation B-5, which is the net momentum of the flux though the control volume. We again divide by ΔV and let $\Delta x, \Delta y, \Delta z \rightarrow 0$:

$$\begin{aligned} \lim_{\Delta x, \Delta y, \Delta z \rightarrow 0} \frac{\iint_{\text{control surface}} \rho \mathbf{v}(\mathbf{v}\mathbf{n})dA}{\Delta V} = & \mathbf{v} \left[\frac{\partial}{\partial x} (\rho v_x) + \frac{\partial}{\partial y} (\rho v_y) + \frac{\partial}{\partial z} (\rho v_z) \right] + \\ & + \rho \left[v_x \frac{\partial \mathbf{v}}{\partial x} + v_y \frac{\partial \mathbf{v}}{\partial y} + v_z \frac{\partial \mathbf{v}}{\partial z} \right] \end{aligned} \quad \text{B-8}$$

B-8 together with the continuity equation B-3 gives:

$$\lim_{\Delta x, \Delta y, \Delta z \rightarrow 0} \frac{\iint_{\text{control surface}} \rho \mathbf{v}(\mathbf{v}\mathbf{n})dA}{\Delta V} = -\mathbf{v} \frac{\partial \rho}{\partial t} + \rho \left[v_x \frac{\partial \mathbf{v}}{\partial x} + v_y \frac{\partial \mathbf{v}}{\partial y} + v_z \frac{\partial \mathbf{v}}{\partial z} \right] \quad \text{B-9}$$

The last term in equation B-5 is the time rate of change of momentum within the control volume, which similarly to the other terms becomes:

$$\lim_{\Delta x, \Delta y, \Delta z \rightarrow 0} \frac{\frac{\partial}{\partial t} \iiint_{\text{control volume}} \rho \mathbf{v}dV}{\Delta V} = \frac{\partial}{\partial t} \frac{\rho \mathbf{v} \Delta V}{\Delta V} = \frac{\partial}{\partial t} \rho \mathbf{v} = \rho \frac{\partial \mathbf{v}}{\partial t} + \mathbf{v} \frac{\partial \rho}{\partial t} \quad \text{B-10}$$

Equations B-5, B-7, B-9 and B-10 are now put together and the x-component is:

$$\rho \left[\frac{\partial v_x}{\partial t} + v_x \frac{\partial v_x}{\partial x} + v_y \frac{\partial v_x}{\partial y} + v_z \frac{\partial v_x}{\partial z} \right] = \rho g_x + \frac{\partial \sigma_{xx}}{\partial x} + \frac{\partial \tau_{yx}}{\partial y} + \frac{\partial \tau_{zx}}{\partial z} \quad \text{B-11}$$

The left hand side is basically the substantial time derivative of the velocity and the equation can thus be written as:

$$\rho \frac{Dv_x}{Dt} = \rho g_x + \frac{\partial \sigma_{xx}}{\partial x} + \frac{\partial \tau_{yx}}{\partial y} + \frac{\partial \tau_{zx}}{\partial z} \quad \text{B-12}$$

The equation B-12 is similar for y and z and the whole system becomes:

$$\rho \frac{Dv_i}{Dt} = \rho g_i + \frac{\partial \sigma_{ii}}{\partial i} + \frac{\partial \tau_{ji}}{\partial j} + \frac{\partial \tau_{ki}}{\partial k}, \text{ where } i, j \text{ and } k \text{ is } x, y \text{ and } z \quad \text{B-13}$$

and not equal.

We want to combine equation B-13 with Newton's law of viscosity, which reads:

$$\text{Shear stress} = \text{viscosity} * \text{rate of shear strain} \quad \text{B-14}$$

Viscosity is a measure of a fluid's resistance to deformation rate and depends on temperature, molecular weight, parameters in the Lennard-Jones potential etc. Shear stresses with x-direction as normal relates to viscosity as:

$$\tau_{yx} = \tau_{xy} = \mu \left(\frac{\partial v_x}{\partial y} + \frac{\partial v_y}{\partial x} \right), \text{ where } \mu \text{ is the viscosity and } \tau_{yx} \quad \text{B-15}$$

is the shear stress in y - direction with x - direction as normal.

The other components look the same with changed subscripts.

Normal stresses relates to the viscosity as:

$$\sigma_{xx} = \mu \left(2 \frac{\partial v_x}{\partial x} - \frac{2}{3} \nabla \mathbf{v} \right) - P, \text{ where } \sigma_{xx} \quad \text{B-16}$$

is the normal stress in x - direction and P is the pressure.

The other components look the same with changed subscripts.

It is now time to combine B-13 with these relations for the viscosity and we get:

$$\rho \frac{Dv_i}{Dt} = \rho g_i + \frac{\partial P}{\partial i} + \frac{\partial}{\partial i} \left(\frac{2}{3} \mu \nabla \mathbf{v} \right) + \nabla \cdot (\mu \nabla v_i) \text{ where } i=x, y, z \quad \text{B-17}$$

B-17 is the Navier-Stokes equations for a fluid.